Palacký University Olomouc, Faculty of Science,
Department of Geoinformatics

Paris Lodron University Salzburg, Faculty of Natural Sciences,
Department of Geoinformatics

ANALYSIS AND 3D VISUALISATION OF WILDFIRES USING EARTH OBSERVATION DATA

Diploma thesis

Author

Opeyemi Kazeem-Jimoh

Supervisor (Palacký University Olomouc)

RNDr. Jan Brus, Ph.D.

Co-supervisor (Paris Lodron University Salzburg)

Prof. Dr. Stefan LANG

Erasmus Mundus Joint Master Degree Programme
Copernicus Master in Digital Earth
Specialization Track Geovisulaization & Geocommunication
Olomouc, Czech Republic, 2024

Palacký University
Olomouc

With the support of the
Erasmus+ Programme
of the European Union

ANNOTATION

This thesis aims to evaluate the possibility of integrating remote-sensing data into advanced 3D visualization and animation. The primary objective is to develop and document a comprehensive workflow for the modeling and rendering of wildfire parameters derived from remote sensing within a 3D environment, with the 2023 Maui Island Fires serving as a case study. The research encompasses an evaluation of the applicability of satellite-derived active fire points and Aerosol Optical Depth (AOD) data, which represent smoke plumes, in the retrospective modeling of wildfire spread. In addition, various satellite datasets and supplementary real-time visual media are utilized to construct an advanced 3D modeling workflow. The thesis details the entire process, from data preprocessing through modeling and animation, culminating in post-processing and video editing. The final output includes five distinct video animations, each depicting the wildfire spread from different perspectives. The effectiveness of the workflow is assessed by comparing the animations with an official fire progression report, leading to a discussion on the successes and challenges associated with the datasets and the developed workflow.

KEYWORDS

Keywords – 3D modeling, Blender, Google Photorealistic 3D Tiles, Flythrough, Animation.

Number of pages: 79

Number of appendixes: 3

This thesis has been composed by *Opeyemi Kazeem-Jimoh* for the Erasmus Mundus Joint Master's Degree Program in Copernicus Master's in Digital Earth for the academic years 2022/2023 and 2023/2024 at the Department of Geoinformatics, Faculty of Natural Sciences, Paris Lodron University Salzburg, and Department of Geoinformatics, Faculty of Science, Palacký University Olomouc. The thesis was supported by the Czech Science Foundation project no. 23-06187S - Identification of barriers in the process of communication of spatial socio-demographic information.

Hereby, I declare that this piece of work is entirely my own, the references cited have been acknowledged, and the thesis has not been previously submitted to the fulfillment of the higher degree.

Palacký University Olomouc
Faculty of Science
Academic year: 2023/2024

ASSIGNMENT OF DIPLOMA THESIS

(project, art work, art performance)

Name and surname:	Opeyemi Adeshewa KAZEEM-JIMOH
Personal number:	R220760
Study programme:	N0532A330010 Geoinformatics and Cartography
Work topic:	Analysis and 3D Visualization of wildfires using Earth Observation Data.
Assigning department:	Department of Geoinformatics

Theses guidelines

The main aim of the thesis is to analyse the possibilities of creating advanced 3D visualizations of wildfires using Earth observation data with a combination of the elevation data. The study will analyse retrospective fire detection using MODIS/VIIRS sensors and satellite-derived smoke detection atmospheric aerosol data (VIIRS Deep Blue Aerosol). The aim is to find a suitable workflow for incorporating thematic layers with elevation data into the rendered 3D scenes. Following appropriate analysis of the various satellite data components, the main visualization workflow will be made in Blender software. Maui wildfires of 2023 will be used as the case study. This work will also test the possibilities of creating animated scenes from the created visualizations. The primary thesis outcome will be several 3D visualizations with textual information explaining the phenomena.

Extent of work report:	max. 50 pages
Extent of graphics content:	as needed
Form processing of diploma thesis:	electronic
Language of elaboration:	English

Recommended resources:

Adab, H., Kanniah, K. D., & Solaimani, K. (2013). Modeling forest fire risk in the northeast of Iran using remote sensing and GIS techniques. *Natural Hazards*, *65*(3), 1723–1743. https://doi.org/10.1007/s11069-012-0450-8

Bowman, D. M. J. S., Williamson, G. J., Abatzoglou, J. T., Kolden, C. A., Cochrane, M. A., & Smith, A. M. S. (2017). Human exposure and sensitivity to globally extreme wildfire events. *Nature Ecology and Evolution*, *1*(3). https://doi.org/10.1038/s41559-016-0058

Castrillón, M., Jorge, P. A., López, I. J., Macías, A., Martín, D., Nebot, R. J., Sabbagh, I., Quintana, F. M., Sánchez, J., Sánchez, A. J., Suárez, J. P., & Trujillo, A. (2011). Forecasting and visualization of wildfires in a 3D geographical information system. *Computers and Geosciences*, *37*(3), 390–396. https://doi.org/10.1016/j.cageo.2010.04.011

Hu, J., Lv, Z., Yuan, D., He, B., & Yan, D. (2023). Intelligent Fire Information System Based on 3D GIS. *Virtual Reality and Intelligent Hardware*, *5*(2), 93–109. https://doi.org/10.1016/j.vrih.2022.07.002

Kim, S., Jeong, Y., Youn, Y., Cho, S., Kang, J., Kim, G., & Lee, Y. (2021). A Comparison between Multiple Satellite AOD Products Using AERONET Sun Photometer Observations in South Korea: Case Study of MODIS, VIIRS, Himawari-8, and Sentinel-3. *Korean Journal of Remote Sensing*, *37*(3). https://doi.org/10.7780/kjrs.2021.37.3.14

Loría-Salazar, S. M., Sayer, A. M., Barnes, J., Huang, J., Flynn, C., Lareau, N., Lee, J., Lyapustin, A., Redemann, J., Welton, E. J., Wilkins, J. L., & Holmes, H. A. (2021). Evaluation of Novel NASA Moderate Resolution Imaging Spectroradiometer and Visible Infrared Imaging Radiometer Suite Aerosol Products and Assessment of Smoke Height Boundary Layer Ratio During Extreme Smoke Events in the Western USA. *Journal of Geophysical Research: Atmospheres*, *126*(11). https://doi.org/10.1029/2020JD034180

Lu, X., Zhang, X., Li, F., Cochrane, M. A., & Ciren, P. (2021). Detection of fire smoke plumes based on aerosol scattering using viirs data over global fire-prone regions. *Remote Sensing*, *13*(2), 1–22. https://doi.org/10.3390/rs13020196

Shennan, K., Stow, D. A., Nara, A., Schag, G. M., & Riggan, P. (2023). Geovisualization and Analysis of Landscape-Level Wildfire Behavior Using Repeat Pass Airborne Thermal Infrared Imagery. *Fire*, *6*(6). https://doi.org/10.3390/fire6060240
Thöny, M., Schnürer, R., Sieber, R., Hurni, L., & Pajarola, R. (2018). Storytelling in interactive 3D geographic visualization systems. *ISPRS International Journal of Geo-Information*, *7*(3). https://doi.org/10.3390/ijgi7030123
Yang, Z., Li, J., Hyyppä, J., Gong, J., Liu, J., & Yang, B. (2023). A comprehensive and up-to-date web-based interactive 3D emergency response and visualization system using Cesium Digital Earth: taking landslide disaster as an example. *Big Earth Data*. https://doi.org/10.1080/20964471.2023.2172823

Supervisors of diploma thesis: **RNDr. Jan Brus, Ph.D.**
Department of Geoinformatics

Date of assignment of diploma thesis: **December 4, 2023**
Submission deadline of diploma thesis: **May 20, 2024**

L.S.

doc. RNDr. Martin Kubala, Ph.D.
Dean

prof. RNDr. Vilém Pechanec, Ph.D.
Head of Department

Olomouc December 4, 2023

CONTENT

LIST OF ABBREVIATIONS

This is a list of abbreviations used in this thesis document.

Abbreviation	**Meaning**
AOD	Aerosol Optical Depth
CAMS	Copernicus Atmosphere Monitoring Service
EO	Earth Observation
EWE	Extreme Wildfire Event
FEMA	Federal Emergency Management Agency
FRP	Fire Radiative Power
MODIS	Moderate Resolution Imaging Spectroradiometer
NASA	National Aeronautics and Space Administration
NDVI	Normalized Difference Vegetation Index
NDWI	Normalized Difference Water Index
NMDI	Normalized Multi-Band Drought index
PDC	Pacific Disaster Center
TIRS	Thermal Infrared Sensor
VARI	Visible Atmospherically Resistant Index
VIIRS	Visible Infrared Imaging Radiometer Suite
WUI	Wildlife Urban Interface

INTRODUCTION

Wildfires (bush fires, forest fires, etc.) though invaluable to vegetative nutrient transfer and development have proven in recent years to have intensified in both unpredictability and destructive capacity. Research has shown that a generally warmer climate and unprecedented weather patterns attributable to climate change have facilitated the occurrence of longer-burning, more intensive, and frequent wildfires culminating in significant loses in biodiversity, not to mention significant human economic loses (Bowman et al., 2017). There also exists a clear variation between disastrous and non-disastrous wildfire events with the most extreme of the latter being categorized as Extreme Wildfire Events (EWE) (Tedim et al., 2018). EWEs are fires that are reported to be significantly economically, socially, and environmentally disastrous.

Understanding the pattern and impact of these wildfires is necessary for rebuilding and rehabilitation to occur. 2023 saw an estimated 4 billion dollars' worth of global economic damage from wildfires, with the cost of rebuilding often being more significant than this. For the 2023 fires in Maui alone, an estimated 5 billion dollars is required for rebuilding efforts (PDC, FEMA, 2023). To undertake the process of rebuilding, it is therefore necessary to visually depict the spread and pattern of destruction.

For this purpose, Earth observation offers an invaluable resource for holistic analysis of wildfire indicators before, during, and after an extreme wildfire event. Factors such as burn area (Long-Fournel et al., 2014), smoke plumes, wind direction, and active fire points as visible using satellites and sensors and may be measured to better understand the contributing factors and damage from such events. Significant research has gone into modeling fire risk to initiate anticipatory action against the onset of wildfires and improve emergency preparedness. Others have also investigated accurately depicting post-fire impact using remotely sensed attributes. This current study aims to retrospectively illustrate the pattern of occurrence of an extreme wildfire event in a 3D environment using such accurately measured EO-derived indicators as the Aerosol Optical Depth (AOD) to depict smoke plumes and sub-daily observations of active fire locations from MODIS. Through this, we hope to recreate the commencement and spread of the Maui Wildfires of 2023. For better understanding and relatability, this will be done using advanced 3D modeling software to better support rebuilding and rehabilitation efforts for this and similar fires.

1 OBJECTIVES

This diploma thesis aims to develop and document a workflow for modeling and rendering remote-sensing derived wildfire parameters in an advanced 3D modeling platform. Furthermore, the suitability of representing smoke plumes in a 3D model of a wildfire, with satellite-derived aerosol optical depth data will be evaluated. The objective of this study therefore is as follows.

i. Develop the workflow for modeling and visualizing real-time and remote-sensing-derived parameters in a 3D environment for retrospective monitoring of a wildfire event.
ii. Identify potential issues with applying remote-sensing-derived parameters of a wildfire in a 3D modeling environment.
iii. Evaluate the viability of using satellite-derived Aerosol Optical Depth in representing smoke plumes in a 3D modeling environment.
iv. Document processes and workflows developed for easy replication and utilization.

2 STATE OF THE ART

Wildfire, Types and Causes.

Wildfires are not only destructive forces, but a natural requirement for the balance maintenance of certain ecosystems, as certain Flora and fauna have developed to adapt to periodic wildfire breakouts especially as they are vital for their ecology. Wildfires often refer to large uncontrolled fires that consume vast amounts of forest or grass land often in rural or peri-urban areas. Historically, wildfires developed to help ecosystems thrive by burning off excess undergrowth and clearing out dead organic matter to support a regenerative process in the ecosystem. However, recent years have seen the proliferation of larger, more frequent, and devastating fires, a phenomenon referred to in literature as Extreme Wildfire Events (EWE). Reasons for these may be natural or anthropogenic but is usually an interplay of both. Human suppression of naturally occurring periodic burns in peri-urban and forested areas has resulted in major pileups of dead wood which serves as ready fuel for more intensive and longer-lasting fires. Climate change has also resulted in dryer temperatures which further aid the drying of dead wood and shrubs to fuel the next major fires. The increase in frequency of such EWEs also leads to a vicious cycle as wildfire in turn generates more carbon emissions thereby fueling the climate change phenomena. According to Copernicus Atmosphere Monitoring Service (CAMS), as of December 10, 2022, global wildfires and vegetation fires in the year alone generated around 1,455 megatons of carbon emissions. At a global scale, they recorded a declining trend in emissions concerning land use changes and declining savanna fires in the tropics, while observing significantly increased fire emissions in different parts of the world, where hotter and drier conditions are leading to increased flammability of the vegetation.

Research has also shown that the socio-economic impacts of EWEs have also increased in recent times. This is attributable to human-induced land use change. We have seen a continuous expansion of human settlement into previously forested regions thereby causing an expansion of peri-urban or Wildland Urban Interface (WUI) (Thomas et al., 2022). There exists a positive correlation between wildfire occurrence in such regions and the socio-economic costs. Socio-economic costs include lost infrastructure and homes, health costs, and other losses from overall economic and business disruptions not to mention loss of lives. The Wildland Urban Interface as defined by (Stewart et al., 2007) “is an area where houses exist at more than 1 housing unit per 40 acres and: 1) wildland vegetation covers more than 50% of the land area or 2) wildland vegetation covers less than 50% of the land area, but a large area (over 1,235 acres) covered with more than 75% wildland vegetation is within 1.5 miles”. It is important to note the significance of these regions to wildfire management because 1) Increased human presence in WUI will result in more human-induced ignitions 2) wildfires in this region have greater human and socio-economic impact.

Over the past 2 decades, there has been a rising trend in costs associated with wildfires with 2017 seeing the highest value as illustrated in Figure 1.

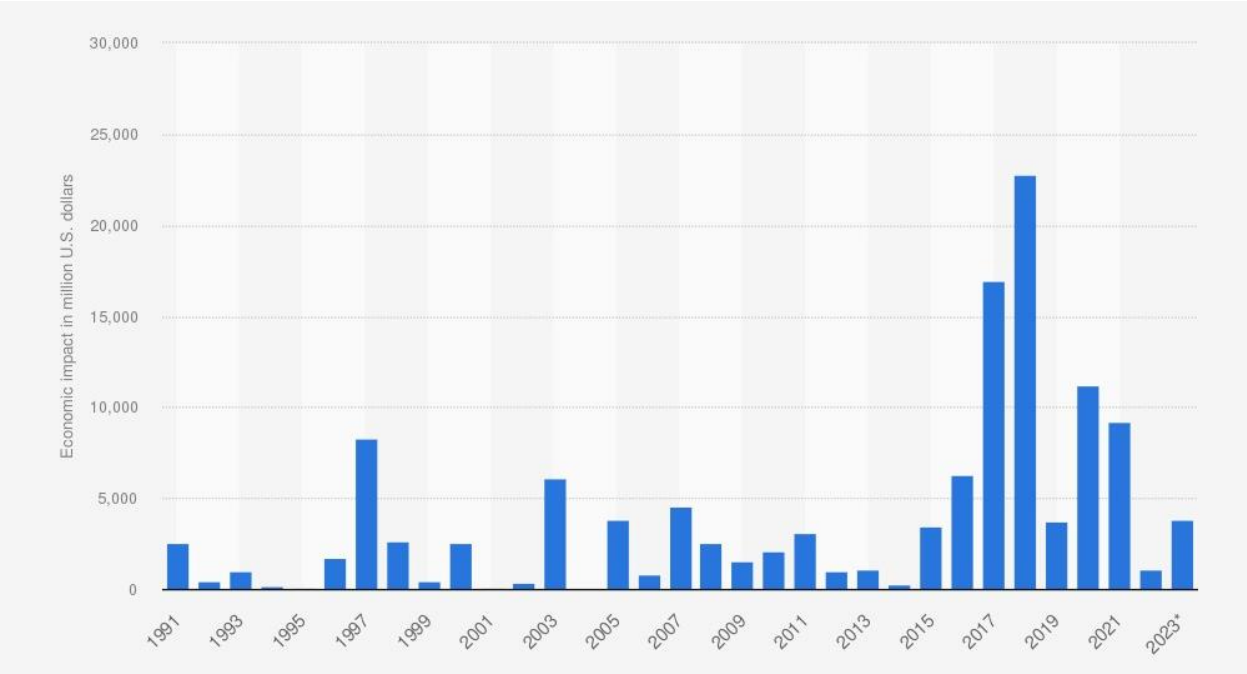

Figure 1 *Economic Damages caused by wildfires globally from 1990 to 2023 (in million U.S. dollars).* (Statista, 2023)

Anthropogenic Ignition and Non-anthropogenic ignition

Talking about wildfires with the most impact on human life, we must also consider the relationship between wildfire causes, the size and magnitude of the fires, and their resulting impact on human life. Wildfires like any fire must be ignited. Historically, periodic fires have been ignited by lightning during thunderstorms. However, there has been an increasing trend in fires caused by human activity. This has given rise to the term "anthropogenic ignitions". As mentioned in the section above, the increasing presence of humans in the WUI as well as anthropogenic-oriented land-use changes have an impact on the increasing number of anthropogenic ignition wildfires. Certain peculiarities have also been observed related to human ignitions and the tenure and type of the resulting wildfire. In their study of characteristics of wildfires in the conterminous US in terms of fire radiative power (FRP)-based fire intensity, event size, burned area, frequency, season length, and ignition type data from > 1.8 million government records and remote sensing data at a 50-km resolution between 1984 and 2016 (Cattau et al., 2020) found that at a national scale, wildfires occur over longer fire seasons (17% increase) and have become larger (78%) and more frequent (12%). Human ignitions have also increased 9% proportionally and such areas dominated by human ignitions experience fires that are twice as frequent and have a fire season that is 2.4

times longer while areas dominated by lightning ignitions experience fires that are 2.4 times more intense and 9.2 times larger. Anthropogenic ignitions are also peculiar in that while lightening-ignitions typically occur within a limited window of time when climatic conditions are conducive to producing thunderstorms, due to their very nature, anthropogenic ignitions occur at any time of year and under a wider range of conditions.(Cattau et al., 2020)

Role Of Remote Sensing and Earth Observation in Monitoring Wildfires (Predictive And Retrospective)

Satellite remote sensing, an advanced Earth observation method, offers extensive data for global change detection by capturing Earth's surface details. It effectively captures the fire regime, a crucial aspect of forest ecosystems, through biophysical measurements. Compared to other methods, remote sensing excels in continuous wildfire monitoring across vast, high-risk, and remote territories. This technology significantly enhances our understanding of environmental dynamics and aids in proactive wildfire management and ecosystem preservation. (Avila-Flores et al., 2010; Hwang et al., 2023; Li et al., 2024; Szpakowski & Jensen, 2019). These measurements are utilized across three phases of wildland fires: pre-fire, fire occurrence, and post-fire. This translates to their application in fire risk assessment, active fire detection, mapping burned areas, and monitoring vegetation recovery (Li et al., 2024; White et al., 2023)

In terms of pre-fire risk management systems, remote sensing plays a vital role in providing variables that feed into various fire risk monitoring models. Certain prominent fire risk rating systems such as Canadian Forest Fire Danger Rating System (CFFDRS) Wildland Fire Assessment System (WFAS), McArthur Forest Fire Danger Rating System (FFDRS), etc. depend on meteorological data such as air temperature, humidity, wind speed and precipitation alone to predict the possibility of ignition and potential damage from a wildfire event, such input is usually subject to data availability across a network of weather stations to which interpolation technique need to be applied to achieve consistent coverage across areas.(Li et al., 2024; Szpakowski & Jensen, 2019). In recent years, however, fire risk assessment models have been developed to overcome the issue of interpolation, by simply leveraging satellite-based remote sensing data as input. The availability and consistency of remote sensing products such as MODIS and VIIRS, as well as optical satellite data from Landsat and Copernicus have enabled the development and use of these remote-sensing-based fire risk indicators. Optical imagery-derived vegetation indices such as NDVI, NDWI, VARI, and NMDI have been compared to measure Fuel Moisture Content, a key variable in wildfire risk estimation. (Avila-Flores et al., 2010; Hwang et al., 2023; Li et al., 2024; Lu et al., 2021; Shi et al., 2024)

Identifying active fire locations in real-time has also become readily available through remote sensing. Smoke plumes and fire spots are two important signals for active fire detection. They can be deduced through the information derived from the following remote sensing platforms not limited to NOAA/AVHRR, MODIS sensor onboard Terra/Aqua, Meteosat Second Generation

Spinning Enhanced Visible and Infra-red Imager, (MSG-SEVIRI), FengYun (FY) Meteorological Satellites, Geostationary Operational Environmental Satellite (GEOS), Himawari-8. Methods used in detection vary form multispectral methods developed from NOAA/AVHRR to an array of algorithms developed in response to the launch of NASA's AQUA and TERRA Satellites such as enhanced contextual fire detection algorithm, multi-spectral threshold analysis, back-propagation, neural network, convolution neural network, the combination of K-means clustering and fisher linear discrimination. (Hwang et al., 2023; Szpakowski & Jensen, 2019).

Smoke Plume Detection from Aerosol Optical Depth

Smoke plume detection from wildfires has also been extensively studied using remote sensing. Aerosol Optical Depth (AOD) (or Aerosol Optical Thickness) indicates the level at which particles in the air (aerosols) prevent light from traveling through the atmosphere. Aerosols scatter and absorb incoming sunlight, which reduces visibility. From an observer on the ground, an AOD of less than 0.1 is "clean" - characteristic of a clear blue sky, bright sun, and maximum visibility. As AOD increases to 0.5, 1.0, and greater than 3.0, aerosols become so dense that the sun is obscured. Sources of aerosols include pollution from factories, smoke from fires, dust from dust storms, sea salt, volcanic ash, and smog. (Sundström,2021; Sawyer et al., 2020; VIIRS Atmosphere Science Team, 2023).

AOD is particularly important for estimating air quality and visibility in areas close to far away from wildfire incidents. This is because smoke plumes rarely dissipate at the point of origin but migrate to farther distances causing negative repercussions. Due to its similarity in spectral signature with other phenomena such as dust clouds and bright surfaces, identifying smoke plumes has been a worthy challenge for researchers and remote sensing experts alike(Lu et al., 2021). Although smoke detection from multispectral imagery is possible and is often done, fire smoke is traditionally detected using an aerosol index calculated from spectral contrast changes usually from moderate-resolution satellite sensors, supported by in-situ measurements. analyzed MODIS, AIRS, CALIOP, PFR, ceilometers, FTS, and Brewer data to quantify the properties of the transported smoke plume originating from the massive wildfires near Moscow which were detected in northern Finland on 30 July 2010. (Loría-Salazar et al., 2021) also did an in-depth analysis of aerosol products from NASA's MODIS and VIIRS satellite retrievals over the western USA during August 2013, with special attention to locally generated wildfire smoke and downwind plume structures. They sought to compare the Aerosol Optical Depth (AOD) product with in-situ AErosol RObotic NETwork (AERONET) observations. They found that in general, these products present similar statistical evaluation metrics for the western USA and are useful tools to characterize aerosol loading associated with wildfire smoke.

The Copernicus program has made it possible to access free, Near Real Time (NRT) Aerosol Optical Depth (AOD) products from the Sea and Land Surface Temperature Radiometer (SLSTR) on board the Sentinel-3 A and B satellites, which monitors, in less than three hours, the location,

abundance, and long-range transport of all atmospheric aerosol particles. Although similar coverage and abundance with other AOD products, Sentinel 3 AOD products have been found to be of a lower quality when compared to others. According to the European Organization for the Exploitation of Meteorological Satellites (EUMETSAT., 2020), only the AOD obtained over ocean surfaces has reached '**Preliminary Operational'** status, which means that its scientific quality is approaching the expected requirements and is therefore comparable to other AOD offerings. AOD over land surfaces is still in the process of calibration and its product quality is not yet within the expected requirements. In addition to this, unlike other alternatives, Sentinel 3 aerosol retrieval is exclusively achieved during daytime with solar zenith angles lower than 80 degrees considered. Therefore, night-time observations are not available.

(Kim et al., 2021) performed a comparison between multiple AOD products including MODIS, VIIRS, Himawari-8, and Sentinel-3, and found that although the other performed at per with each other, Sentinel-3 AOD was of a lesser quality.

3D Visualization in Hazard Management

Advances in information technology have made it possible to visualize a wide range of phenomena in virtual reality (augmented reality). A simulation of real-life events is also made possible by such technologies in combination with real-time observations from earth monitoring systems made possible by remote sensing. Several examples exist in literature where mainstream 3D modeling technologies such as Blender, and more dedicated 3D GIS technologies like Cesium and Google Earth have been used to better understand the origin and impact of diverse disaster types, by intuitively and interactively presenting multisource geographic and remote sensing data from disaster events and further expert knowledge to decision-makers and the general public in an easily understandable manner. Such technologies have also been used both in pre-disaster monitoring and in disaster emergency management systems to greatly improve response effectiveness and aid rehabilitation efforts post-disaster (Hu et al., 2023).

(Thöny et al., 2018) explored the importance of 3D visualization in dynamic and intuitive geospatial story telling as it is invaluable for passing across vital expert geospatial information, especially to non-expert users such as decision-makers and the public. (Yang et al., 2023) developed a comprehensive Web-based 3D Web GIS platform for Emergency Response using the Vue.js web application framework and Cesium API taking a landslide event as an example. (Shennan et al., 2023) developed and evaluated the effectiveness of 3D Geovisulaization tools for analyzing wildfire behavior while studying portions of the Thomas and Detwiler wildfire events that occurred in California in 2017. Fire features such as active fire fronts and rate of spread (ROS) vectors derived from repetitive airborne thermal infrared (ATIR) imagery sequences were incorporated into Geovisulaization tools hosted in a web GIS application. (Song & Duveneck., 2008) evaluated the use of Visual Nature Studio, a 3D terrain visualization software in visualizing a wildfire in the New Jersey Pine Barrens based on available GIS and forest inventory data. Inputs

included a digital elevation map, orthophotos for visualizing surface features such as roads and buildings, Image models for vegetation constructed from digital photos of actual species edited in Photoshop, Forest ecosystems created using the image models linked with the forest inventory data, and fire visualization performed using shapefiles for fire spread and intensity provided by the FARSITE model with the resulting visualization provided both still frame and animated views of the wildfire.

Even active fire emergency response models are being developed with the help of 3D GIS. (Hu et al., 2023) developed an intelligent Fire rescue platform based on 3D GIS and IoT, with a focus on solving the problem of rescue vehicle scheduling and the evacuation of trapped persons in the process of fire rescue. (Castrillón et al., 2011) also developed a wildfire forecasting and monitoring platform, which incorporates a 3D virtual environment and a fire simulation engine. Also using the FARSITE simulation model, the tool allows users to simulate and visualize fire spread across terrain, incorporating spatial data on topography and vegetation alongside weather and wind information simultaneously.

Blender as a Tool for Geospatial 3D visualization.

Blender is a powerful and versatile free and open-source 3D computer graphics software toolset, initially released in 1998 by Ton Roosendaal as an in-house application for the Dutch animation studio NeoGeo. It runs on multiple operating systems, including Windows, macOS, Linux, BSD, and Haiku. Blender's extensive features include 3D modeling, sculpting, texturing, rigging, animation, rendering, compositing, motion tracking, video editing, and game creation. Its ability to handle complex tasks makes it popular among professionals and hobbyists alike in various fields such as animation, visual effects, video games, and architectural visualization. Blender also supports a broad range of plugins and scripts to enhance its functionality, fostering a vibrant community of developers and users who continuously contribute to its development and improvement.

Although 3D visualization of geospatial data is increasingly gaining popularity in recent times, this has mostly been done in dedicated GIS-enabled 3D software like Cesium, which is considered more limited in advanced 3D modeling compared to other dedicated platforms. Table 1 illustrates some of the advantages of Blender over cesium, while table 2 compares Blender to other mainstream 3D modeling suites. Blender has been increasingly utilized in geospatial projects due to its robust modeling, texturing, and rendering capabilities. Thanks to the incorporation of Blender’s native python interface and certain spatially oriented plugins in Blender like BlenderGIS (domes, n.d.), spatial data ingestion and handling within the Blender space is now possible. However, there are still some areas of concern when working with spatial data in Blender, particularly concerning Coordinate reference systems (Ordinance Survey UK, 2024). Specialized packages such as GDAL, and OGR, among others, which mainstream GIS software leverage is absent in mainstream advanced modeling software. (Southall & Biljecki, 2017) examined the

application of the VI-Suite for environmental analysis and simulation. Their findings indicated that the free and open-source characteristics of the VI-Suite, along with the utilization of Blender mesh geometry to specify calculation points, have led to usage scenarios beyond the authors' original intentions, such as extensive urban shadow and radiation analyses. This mesh-based method's flexibility allows for the analysis of large geospatial datasets by providing users with detailed control over the placement of calculation points within the model. Blender has also been used in conjunction with PostGIS to create and structure 3D GIS data models. The integrative approach highlighted allows for the detailed modeling of complex scenes and the seamless integration of 3D models with GIS data, enhancing spatial analysis and visualization capabilities (Scianna, 2013). Blender's ability to handle and visualize large-scale geospatial data sets has been demonstrated in projects focused on urban planning. By importing real-world geospatial data into Blender, users can create accurate 3D models of urban environments for analysis and presentation purposes (Ordinance Survey UK, 2024). Blender has also been employed as a teaching tool for 3D Geovisulaization. (Tateosian & Tabrizian, 2017) found that the use of Blender along with SketchFab in educational settings helps students understand complex spatial data and develop skills in 3D modeling and visualization.

Feature	**Blender**	**Cesium**
Open Source	*Yes*	*No*
Spatial Data Handling	*Limited*	*Advanced*
Ease of Use	*Moderate Learning Curve*	*User-friendly for geospatial data*
Cost	*Free*	*Subscription plans*
3D Modelling Capability	*Advanced*	*Limited to geospatial applications*
Animation Capability	*Advanced*	*Basic*
Community Support	*Large and active community providing tutorials, plugins, and support.*	*Smaller, specialized community focused on geospatial applications.*
File Format Support	*Supports a wide range of 3D file formats including .obj, .fbx, .gltf, and also georeferenced 3D tiles.*	*Also supports mainstream model formats like .gltf, but also georeferenced data formats like 3D Tiles.*
Learning Resources	*Extensive learning resources including official documentation, tutorials, and courses.*	*More limited learning resources, primarily focused on geospatial data handling.*

Table 1 *Comparing Blender to GIS-enabled 3D software Cesium.*

Feature	**Blender**	**Autodesk Maya**	**Autodesk 3ds Max**	**Cinema 4D**
Open Source	*Yes*	*No*	*No*	*No*
Performance	*High, good for diverse tasks*	*High, excel in animation*	*High, Excels in modeling*	*High, good all-round*
Ease of Use	*Moderate learning curve*	*Steeper Learning Curve*	*Moderate Learning curve/User friendly*	*Intuitive and easy to learn*
Cost	*Free*	*Subscription-based*	*Subscription-based*	*Subscription-based*
3D Modelling Capability	*Advanced*	*Advanced with comprehensive tools*	*Advanced, best for modeling*	*Advanced, Versatile*
Animation Capability	*Advanced*	*Best for character animation*	*Good. But this is a secondary focus*	*Good, suitable for diverse types*
Rendering Capability	*Advanced*	*Advanced*	*Advanced*	*Advanced, fast, and efficient*

Table 2 *Comparison to other major 3D modeling software.*

3 METHODOLOGY

3.1 Study Area and Context

Situated in the northwestern part of the Hawaiian archipelago, Maui spans 735 square miles (1,883 km²). It is the second-largest island in the archipelago and ranks 17th in size in the United States. Maui's daytime temperatures are warm year-round ranging from 75 °F (24 °C) to 90 °F (32 °C). The island features a variety of climatic conditions, each unique to its sub-regions. These sub-regions are defined by major physiographic features (such as mountains and valleys) and by location on the windward or leeward side. Since half of the land is within 5 miles (8 km) of the coast, the island is also predisposed to a strong marine influence and susceptible to strong winds from hurricane-like weather conditions(Wikipedia, 2024).

South Maui (Kihei, Wailea, and Makena) and West Maui (Lahaina, Kaanapali, and Kapalua) are both on the leeward side. These areas are typically drier, with higher daytime temperatures (up to 92 °F (33 °C)), and the least amount of rainfall. Upcountry Maui is the name for the sloping area on the western face of the Haleakalā Volcano including the towns of Makawao, Pukalani, and Kula. Ranging in altitude between 1500ft and 4500ft, its climate tends toward mild heat (between 70 °F (21 °C) and 80 °F (27 °C)) during the day with cool evenings. (Wikipedia, 2024). Like the rest of Hawaii, the economy of Maui is driven largely by tourism, with construction and agriculture also being prevalent. As of 2017, 40% of the overall GDP of Maui Country (including the islands of Molokai, Lanai, and the uninhabited Kaho'olawe) was accounted for by Tourism. Maui also has a rich history, and one of its most significant historical towns is Lahaina. (Maui County, 2017).

Lahaina is located on the western tip of Maui and is historically significant as a major port during the whaling era. Many historical artifacts from that period were preserved here until the 2023 fires. Of Maui's population of 164,183 in 2024, Lahaina being the 4th most populous settlement has 12,596. On Aug. 8, 2023, wind-driven wildfires on the island of Maui destroyed more than 2,200 structures and caused about $5.5 billion in damages. The most significantly impacted area was the historic district of Lahaina, where more than 100 lives were lost. The August 2023 Maui wildfires now rank as the fifth deadliest in U.S. history and the worst natural disaster in Hawaii's history (Maui Police Department, 2024).

According to the U.S. Drought Monitor, 2023, about 30% of Maui had in the months preceding the fire, been experiencing moderate drought situations, with some places that burned coinciding with areas predicted to be in severe drought. This combined with low humidity and the prevalence of non-native invasive species of vegetation results in dry fire-prone vegetation.

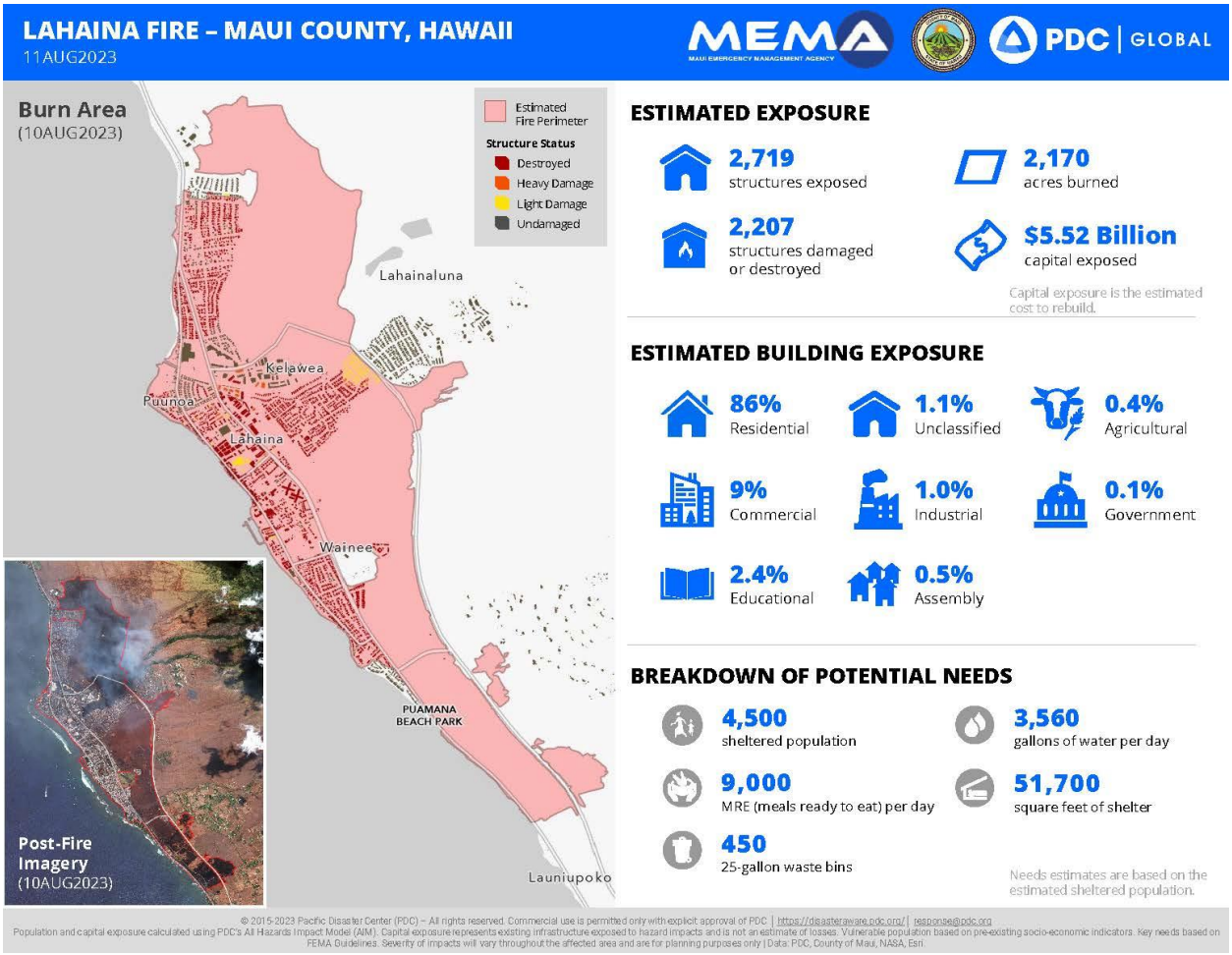

Figure 2. *Initial Post Disaster Impact Assessment* (PDC, FEMA, 2023)

3.2 Data

3.2.1 Active Fire Data

To create a 3D visualization of the progression of the Maui Wildfires using remote sensing data, a review of available remote sensing datasets about fires was done. Prominent among these is the freely available NASA Fire Information for Resource Management System (FIRMS) active fire data set, which has in recent times gained popularity as the major source of satellite-derived detection of active fires. This data, which is in the form of points (latitude, longitude) is derived from Moderate Resolution Imaging Spectroradiometer (MODIS), Visible Infrared Imaging Radiometer Suite (VIIRS), and Landsat Operational Land Imager (OLI) and is available to download in multiple formats. According to (NESDIS and NOAA, n.d.), VIIRS is the successor to MODIS for Earth science data product generation. The 375m I-band data complements the MODIS fire detections; they both show good agreement in hotspot detection but the improved spatial resolution of the 375m data provides a greater response over fires of relatively small areas and provides improved mapping of large fire perimeters. Each hotspot in the dataset represents the approximate center of a 375m pixel area wherein fire was detected (Earth Science Data Systems, 2015).

For the Maui fires of 2023, active fire shapefiles were downloaded for August 8th through 10th, as this is the period when active fire is detected, see Figure 3.

Figure 3 *The active fire spots as detected by NASA FIIRMS on August 8th, 9^{th,} and 10th, 2024.* (NASA-FIRMS, 2023)

With VIIRS having the highest spatial and temporal resolution, active fire data from its joint NASA/NOAA Suomi-National Polar orbiting Partnership (S-NPP) and NOAA-20 (JPSS-1) satellites was downloaded, combined and used for this study. Data from another satellite NOAA-21 (JPSS-2) only became available from 17 January 2024 and is not available for this fire. Although the temporal resolution of each satellite is 2 times per day, some days have up to 3 observations because of the overlap between the satellites and the nearness of the study area to the equator. A total of 540 individual active fire points were detected over the 3 days, broken down into 13 time-steps. This categorization is depicted in Table 3.

Acquisition Date	Actual date coded	Acquisition Time (Original)	Acquisition Time (Local)	Time of Day (Day/Night)
8th	8th	11:45	1:45	N
8th	8th	12:34	2:34	N
8th	8th	22:57	12:57	D
8th	8th	23:46	13:46	D
9th	8th	0:35	14:35 (previous day)	D
9th	9th	11:25	1:25	N
9th	9th	12:14	2:14	N
9th	9th	13:06	3:06	N
9th	9th	23:26	13:36	D
10th	9th	0:18	14:18 (previous day)	N
10th	10th	11:06	1:06	N
10th	10th	11:55	1:55	N
10th	10th	12:46	2:46	N

Table 3 *Active fire spots categorized.*

3.2.2 Digital Elevation Model (DEM)

DEMs are important remote-sensing-derived datasets useful in the 3D modeling of the earth. In this study, the DEM is used to depict real-world elevation in the 3D model. For this, a 10m DEM available through USGS National 3D Elevation Program (3DEP), which is the highest resolution, freely available DEM available for the whole Island of Maui was downloaded from (USGS, n.d.).

3.2.3 Optical Imagery (Texture)

To serve as the texture for the DEM, several options of satellite imagery were initially considered, including Sentinel 2 Cloudless data products, Landsat, and Google Maps Satellite imagery. Because of the high resolution available for the Sentinel 2 Cloudless data (EOX, n.d.), as well as the lack of clouds, it was selected and downloaded through QGIS Quick Map Services (QMS, n.d.) Plugin at 10m spatial resolution and a scale of 1:350,000. This cloudless product is an aggregation of non-cloud pixels from several sentinel 2 images to form a cohesive, quality-assured single image usually spanning the globe. The data used in this study is from 2021. The temporal resolution was deemed suitable because this texture is utilized on a large scale, wherein significant changes to the landscape within the subsequent years would be neither visible nor consequential.

3.2.4 Optical Imagery (Burned Building Analysis)

To assess the building damage in the aftermath of the fire, 33cm Maxar Satellite Imagery was freely obtained for the aftermath of the fire. 5 images were downloaded covering the affected areas over 2 days (August 9th and August 12th, 2023) via the Open Data Program (Maxar, 2023). Because it is available in small granules on the Maxar site, the already mosaiced version from Open Aerial Map (OAM) was downloaded for this study (OAM, 2023). This dataset was also used to validate the fire progression timeline derived from news sources.

3.2.5 Google Photorealistic 3D tiles.

This study sought to 3D visualize the progression of the fire in Lahaina, which was most impacted. To do this a 3D model of the area was required. For this purpose, Photorealistic 3D Tiles (Google, 2024) which are 3D mesh textured with high-resolution imagery, were acquired through the **blosm** Blender plugin (vvoovv, n.d.). The tiles are made available through the public 3D Tiles API. Photorealistic 3D Tiles are in the OGC standard glTF format, which means that renderer that supports the OGC 3D Tiles specification, such as Cesium (Cesium, 2024) and Blender can be used to build 3D visualizations. The imagery used in Google Photorealistic 3D Tiles is acquired through extensive image capture campaigns. These campaigns involve capturing high-resolution imagery, which is then processed using advanced photogrammetry techniques to create detailed 3D models of the world. Google incorporates the following sources to create the tiles: The General Bathymetric Chart of the Oceans; The International Bathymetric Chart of the Arctic Ocean; Columbia University's Lamont-Doherty Earth Observatory; Landsat; Copernicus; Monterey Bay Aquarium Research Institute; Airbus; National Geospatial-Intelligence Agency; National Oceanic and Atmospheric Administration; National Science Foundation; Scripps Institution of Oceanography; School of Ocean and Earth Science and Technology, University of Hawai‘i at Mānoa; U.S. Navy and United States Geological Survey (CNN, 2024).

Upon utilizing these tiles, however, it was observed that for the Lahaina area, the data is not up to date. Certain neighborhoods currently existing in Lahaina such as Kohoma Village, and the Komo Mai street area are not visible in the 3D tiles. Google has not specified the years when these captures are done but promises a continuous coverage campaign to ensure the tiles remain up to date.

Figure 4 *Some developments found in Maxar Satellite Imagery acquired on 12th, August 2024(top), but not in Google's Photorealistic 3D Tiles downloaded on 30th June 2024, in Blender (bottom).*

3.2.6 Other Datasets

Other datasets used include.

1. Manually digitized reference historical sites using Google My Maps
2. Lahaina Area Map digitized in QGIS using the MAUI county digital zoning map as a reference (Eui, 2022).
3. Administrative boundary data from (geoBoundaries, n.d.) refined using Sentinel 2 Cloudless 2021 satellite imagery in QGIS.
4. Lahaina building data clipped from the larger Hawaii OpenStreetMap (OSM) Building data (2020) accessed from Humanitarian Data Exchange (OSM & HUMDATA, 2020). This option was chosen over downloading directly from the OSM website because more buildings are available on the HUMDATA dataset than in the current OSM database.
5. News updates reporting real-time events from the fire were leveraged to piece together a minute-by-minute timeline for modeling the progression of the fire in Lahaina. A full list of sources consulted is listed in table 5.

News Outlet	**Headline**	**URL**
CNN	Everything was on Fire: The hours that brought Lahaina to ruins.	link
NBC News	Timeline: How ferocious wildfires devastated Maui, hour by hour	link
New York Times	Inside the Deadly Maui Inferno: Hour by Hour	link
ABC News	Timeline: How the deadly wildfires took over Maui day by day	link
LA Times	How the Maui Fires consumed Lahaina	link
CBS News	How did the Maui fire start? What we know about the cause of the Lahaina blaze	link

Table 5 *Mainstream news sources consulted for this study.*

3.3 Software

Several separate software was used in performing the different processes that made up the workflow for this study.

3.3.1 Preprocessing

Initial exploration of active fire data and boundary shapefiles was done in ArcGIS Pro and QGIS simultaneously. To prepare the data for modeling in Blender, time steps needed to be converted into frames for animation purposes. This was done in Excel.

3.3.2 3D modelling and Render

The major 3D modeling software used is Blender (version 4.1.1). Although 3D visualization of geospatial data is increasingly gaining popularity in recent times, this has mostly been done in dedicated GIS-enabled 3D software like Cesium, which is considered more limited in advanced 3D modeling compared to other dedicated platforms. On the other hand, Blender's capability for handling real-world geospatial data has, however in recent times been improved with its Google Photorealistic 3D Tiles integration through the ***blosm*** plugin, which has been leveraged in this study. This part of the exercise could only be completed after extensive perusal of tutorials and documentation. Because of Blender's large user community, there exists an abundance of tutorials concerning every aspect of the software, although it is important to note that there are not as many such resources on the use of Blender with geospatial data.

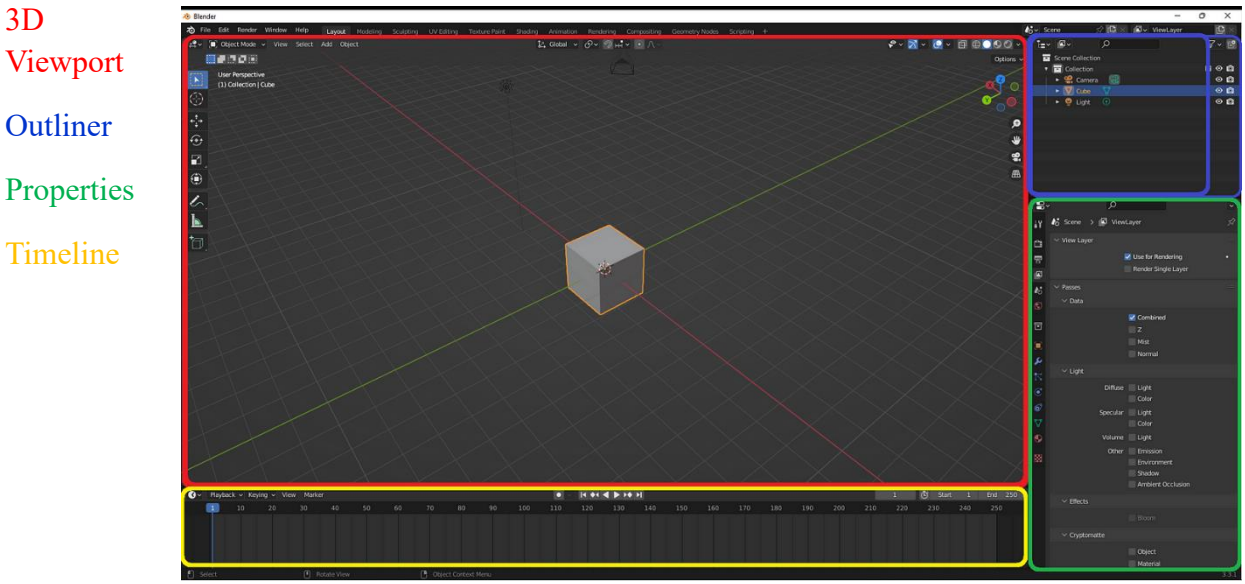

Figure 5 *Blender's Default User Interface.* (Kay, 2022).

3.3.3 Post-processing (Video Editing)

For Video editing and post-processing, Adobe's Premiere Pro was leveraged. This was used to add Titles and Descriptions, Insets, Callouts tags, Timeline, Scalebar, and other cartographic details to the resulting animation. Google Studio was also used to plan flythrough scenes that would later be rendered in Blender.

3.3.4 System Properties

Two different zoom levels are modeled in this study. First is the overview animation depicting the fires across Maui Island (Maui Island Fire Animation). Second is the animation detailing the progression of the fire in Lahaina and its aftermath (Lahaina Fire and Smoke Animation).

For the data gathering and preprocessing, as well as 3D model creation, animation, and rendering of the Maui Island Fire, a computer with CPU INTEL Core i7-4770 BOX (3,4GHz, LGA1150, VGA) 32GB GTX 1070ti, was used. This, however, proved insufficient for the closeup modeling of the fire progression in Lahaina. Another computer with specifications, CPU AMD Ryzen 9 7950X with 16-Core Processor (3.1GHz,1.7GHz) with 128GBRAM using NVIDIA GeForce RTX 4090 Graphics card with 24GB dedicated memory, had to be used for the remaining workflow (mainly for the fire and smoke modeling) including rendering and post-processing.

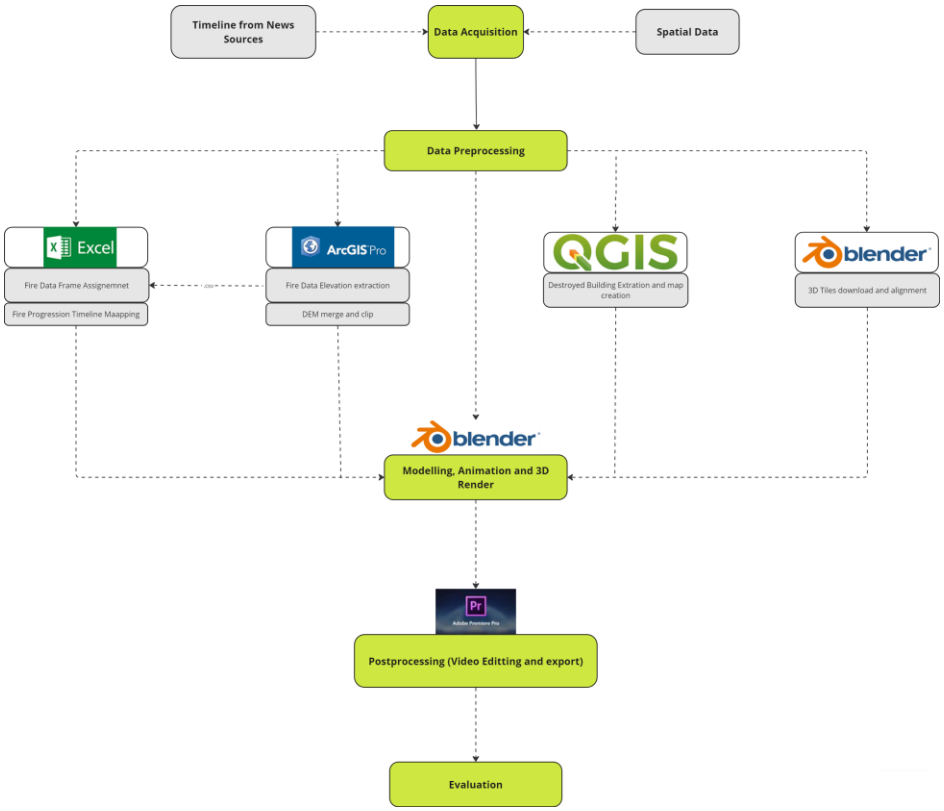

Figure 6 *Workflow Diagram for this study*

4 DATA PREPROCESSING WORKFLOW

Before the Blender workflow could begin, a few steps had to be carried out for the data to be used in the modeling.

4.1 Maui Island Fire Animation

For this level, the datasets required were the 10m DEM, satellite imagery for texture, active fire data, and administrative boundary data.

Firstly, the administrative boundary data had to be improved to better cover the edges of the island, as depicted in Figure 7. This was then used to extract the dimensions of the DEM. The DEM had initially been mosaiced after being downloaded in 3 separate parts. Sentinel 2 cloudless imagery was also downloaded using the "QuickMapServices" plugin in QGIS.

The Active fire data downloaded from the 2 different satellites were merged into 1. For the fire points to have the right elevation on the 3D model, their elevation values were extracted from the DEM using ArcGIS Pro's "Extract Values to Points" tool. To ingest it into Blender, the shapefile was converted to .csv format, which was further manipulated in excel. Time steps were converted into frames for animation in Blender.

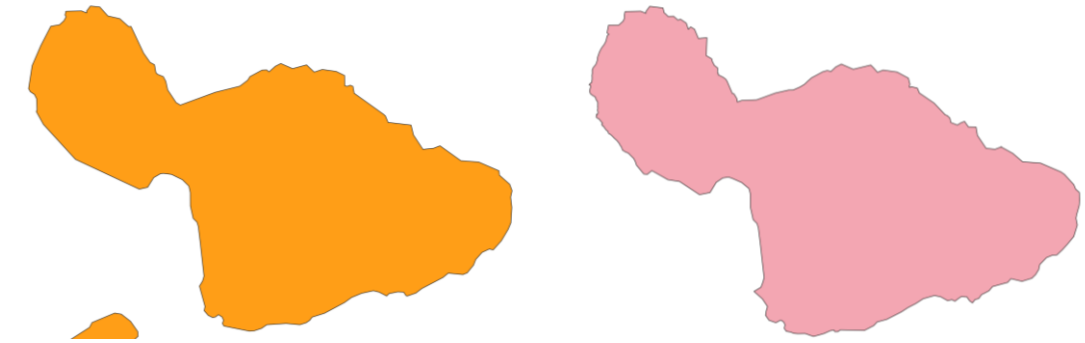

Figure 7 *Maui Island Boundary before (left) and after (right) refinement.*

4.1.1 Dealing with too few time-steps

Initially, each frame represented 1 timestep in the data. Since there are only 13 time steps over the 3 days (5,5,3) of the fire (as captured in the data), there rises the challenge of showing a realistic-looking video animation. In animation, the standard frame rate is 24fps to ensure a realistic-looking playback rate, although this can be adjusted as required. An animation of 1fps was tested however, this was found to be too slow and unrealistic. This necessitated an adjustment in the frame distribution.

A solution to this was to increase the number of frames each time step represents. To do this, each time-step was split into 3 frames. The frame rate was then increased to 3fps, which resulted in a better playback rate as seen in the resulting animation.

Acquisition Date	Actual date coded	Acquisition Time (Original) 24hour	Acquisition Time (Local) 24hour	Initial Frame	Frame used
8th	8th	11:45	1:45	1	16-18
8th	8th	12:34	2:34	2	19-21
8th	8th	22:57	12:57	3	22-24
8th	8th	23:46	13:46	4	25-27
9th	8th	0:35	14:35 (previous day)	5	28-30
9th	9th	11:25	1:25	6	31-33
9th	9th	12:14	2:14	7	34-36
9th	9th	13:06	3:06	8	37-39
9th	9th	23:26	13:36	9	40-42
10th	9th	0:18	14:18 (previous day)	10	43-45
10th	10th	11:06	1:06	11	46-48
10th	10th	11:55	1:55	12	49-51
10th	10th	12:46	2:46	13	52-54

Table 6 *Active fire point data coding. To account for the introduction part in the resulting animation (first 15 frames), the starting frame used for the fire data is 16.*

frame	latitude	longitude	BRIGHT_T3	FRP	RASTERVALU
1	20.80995	-156.29	298.16	12.07	990.4592
1	20.80944	-156.286	310.04	40.95	1042.529
1	20.81046	-156.294	293.48	12.07	930.2388
1	20.80591	-156.291	295.46	23.92	1016.001
1	20.8054	-156.286	299.19	49.67	1007.965
1	20.80642	-156.295	291.82	23.92	940.6693
2	20.80902	-156.292	320.37	79.46	959.5051
2	20.80449	-156.293	291.36	79.46	974.7274
2	20.80537	-156.298	291.86	61.52	917.5107
2	20.81169	-156.305	293.63	11	788.3123
2	20.80726	-156.283	302.52	52.79	1107.338
2	20.80815	-156.288	319.26	79.46	1030.653
2	20.8099	-156.296	318.31	61.52	891.369
2	20.81079	-156.301	311.3	61.52	828.2964
2	20.81355	-156.291	295.96	38.02	968.3506
2	20.81442	-156.295	304.8	29.43	863.8928
2	20.81531	-156.3	294	29.43	806.8176
3	20.80714	-156.299	305.78	10.48	879.9129
3	20.80612	-156.304	304.64	10.48	827.2957
3	20.80946	-156.3	307.3	14.98	838.9597
3	20.80842	-156.305	308.06	14.98	804.3026
3	20.81382	-156.307	307.82	8.75	763.5778
3	20.81028	-156.284	297.3	5.82	1060.695
3	20.80738	-156.283	296.62	7.81	1111.373
3	20.80633	-156.288	298.12	5.42	1007.615

frame	og_frame	latitude	longitude	BRIGHT_T3	FRP	RASTERVAI	code
16	1	20.80995	-156.29	298.16	12.07	990.4592	1.1
16	1	20.80944	-156.286	310.04	40.95	1042.529	
16	1	20.81046	-156.294	293.48	12.07	930.2388	
16	1	20.80591	-156.291	295.46	23.92	1016.001	
16	1	20.8054	-156.286	299.19	49.67	1007.965	
16	1	20.80642	-156.295	291.82	23.92	940.6693	
17	1	20.80995	-156.29	298.16	12.07	990.4592	1.2
17	1	20.80944	-156.286	310.04	40.95	1042.529	
17	1	20.81046	-156.294	293.48	12.07	930.2388	
17	1	20.80591	-156.291	295.46	23.92	1016.001	
17	1	20.8054	-156.286	299.19	49.67	1007.965	
17	1	20.80642	-156.295	291.82	23.92	940.6693	
18	1	20.80995	-156.29	298.16	12.07	990.4592	1.3
18	1	20.80944	-156.286	310.04	40.95	1042.529	
18	1	20.81046	-156.294	293.48	12.07	930.2388	
18	1	20.80591	-156.291	295.46	23.92	1016.001	
18	1	20.8054	-156.286	299.19	49.67	1007.965	
18	1	20.80642	-156.295	291.82	23.92	940.6693	
19	2	20.80902	-156.292	320.37	79.46	959.5051	2.1
19	2	20.80449	-156.293	291.36	79.46	974.7274	
19	2	20.80537	-156.298	291.86	61.52	917.5107	
19	2	20.81169	-156.305	293.63	11	788.3123	
19	2	20.80726	-156.283	302.52	52.79	1107.338	
19	2	20.80815	-156.288	319.26	79.46	1030.653	
19	2	20.8099	-156.296	318.31	61.52	891.369	

Figure 8 *The CSV file before (left) and after (right)the frame readjustment*

It is advised to remove all unnecessary columns from the data, especially columns containing text, as this would affect the ingestion into Blender. Here, only the useful attributes are left such as the coordinates, elevation value, Fire Radiative Power (FRP), and brightness value, although the latter 2 are correlated and only FRP is used.

4.1.2 Smoke Plume Modelling Limitation

An initial objective of this study was to model the smoke plume from the Maui Island fire using remote sensing data, specifically VIIRS Deep Blue Aerosol 6 mins 6KM Swath data, However, upon exploring the available data through NASA's Worldview Online data viewer (NASA, 2023), it was found that the data for Maui was too coarse and almost non-existent. An alternative, the Dark Target AOD product which is also similar in resolution to the Deep Blue was also explored and found to yield slightly better results but still too coarse to effectively model in Blender as smoke. For both products, the sensor/algorithm resolution is 6 km at nadir, the imagery resolution is 2 km at nadir, and the temporal resolution is daily. The resolution is much coarser out toward the edge of the swath. (NASA Data Viewer, 2023).

For reference, a similar animation produced by (Peter Atwood, 2023) utilized a much coarser resolution aerosol data for Canada, which yielded better modeling results.

Below are GIFs showcasing the AOD data availability for the Maui fires, as compared to Canada Fires.

Figure 9 *Deep Blue AOD over Maui Island (8/8/23) SNPP (left), NOAA20/VIIRS (right)*

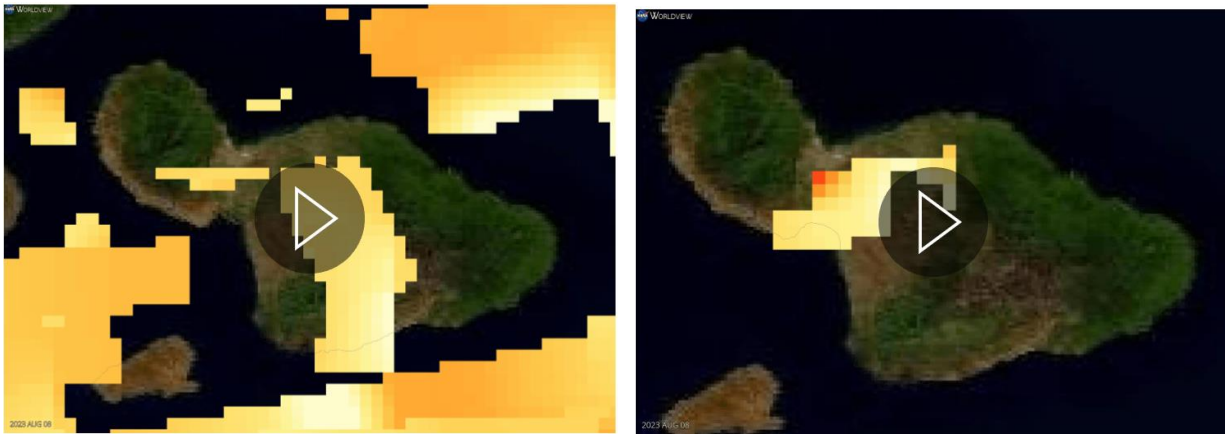

Figure 10 Dark *Target AOD over Maui Island (8/8/23) SNPP (left), NOAA20/VIIRS (right)*

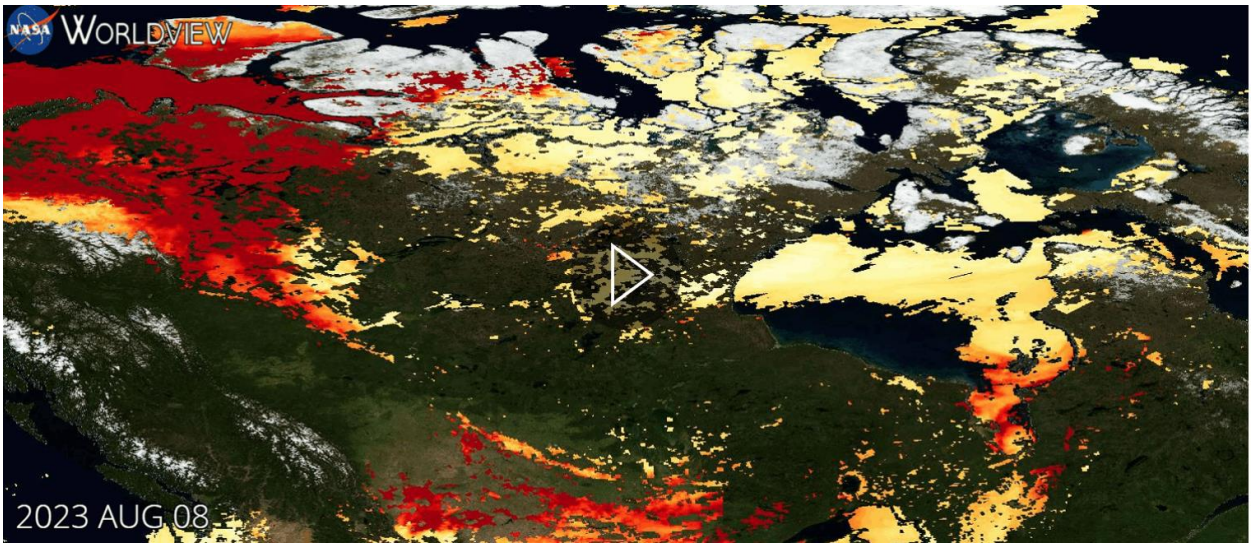

Figure 11 Dark Target AOD over Canada (8/8/23) NOAA20/VIIRS

4.2 Lahaina Fire and Smoke Animation

For this close-up view of the Lahaina Fire, the datasets used are Google's Photorealist 3D tiles, a coded timeline of the fire as observed from news sources and remote sensing data, and 3D fire and smoke material.

4.2.1 Timeline

The main dataset that needed to be compiled in pre-processing was the timeline of the progression of the fire. This was manually pieced together using news sources, available remote sensing sources, and active fire point locations. It is known that the fire in Lahaina spread to most of the burned area within the first 12 hours starting from around 06:27 hours on August 8th (NBC news source) and kept burning/smoking till 11:20 hours on August 9th (Maxar satellite image). Table 7 illustrates this.

Date	Time (approximate)	Fire Progress	Reference
August 8th	06:27 - 14:00	3-acre fire along Lahainaluna Road starts and is extinguished	News Sources (see table 5)
August 8th	14:00 - 15:00	Fire is reignited in a gully from the previous one	News Sources (see table 5)
August 8th	15:00 - 16:00	Fire flares up and travels fast toward neighborhoods along Lahainaluna road	News Sources (see table 5)
August 8th	16:00 - 17:00	Fire has reached Lahaina Central historic district	News Sources (see table 5)
August 8th	18:00 – 19:00	The entire harbor is covered in intense fire and smoke. Aina Nalu Condos on fire.	News Sources (see table 5)
August 8th	19:03	Last live footage consulted. Explosive fire ravages the harbor.	News Sources (see table 5)
August 8th	20:25	Areas still burning were observed in the north and extreme south of Lahaina.	NASA Thermal Sensor
August 9th	01:25	Active fire points	NASA FIIRMS
August 9th	02:14	Active fire points	NASA FIIRMS
August 9th	03:06	Active fire points	NASA FIIRMS
August 9th	11:20	Remnants of smoke and fire in vegetation in the extreme northeast and southeast of the burned area	Maxar Imagery

Table 7 *Timeline of Lahaina Fire Progression*

Although some aspects of the Lahaina fire continued to burn on a smaller scale well into August 10th (NASA FIIRMs) with some fires in other parts if Maui still burning into August 15th (source), the resulting animation is limited to within the first 24 hours of the fire starting in Lahaina, as most of the progression occurred within this time.

Figure 12 *Active fire spots in Lahaina observed by VIIRS on August 10th (captured at 02:14 03:06 and 13:36), over Maxar imagery from 12th August.*

4.2.2 Download Google Photorealistic tiles using the blosm plugin

The 3D model of the area needed for the 3D scene was downloaded via the blosm plugin in Blender. The plugin is freely available to download (although there is a paid tier). It offers a straightforward interface that allows direct download in Blender of any place in the world for which data is available(vvoovv, n.d.).

To save rendering resources and Google maps credits, it is advised to limit downloads of large areas at very high details. For this work, 2 downloads were done, each with varying levels of detail. Table 8 illustrates the parameters used.

Zoom level	Level of detail	Coordinates	Usage
1	Building with more details	-156.68208,20.86783, -156.67010,20.87991	Zoomed-in view showcasing the historical landmarks affected
2	Block of Buildings	-156.69374,20.85641, -156.65838,20.90469	Overview of the entire burn area
3	District		Background Filler

Table 8…*Parameters used to download 3D Photorealistic tiles in Blender.*

Figure 13 *The downloaded tiles as scaled and aligned in Blender. The labels are in yellow.*

4.2.3 Burned Building Footprints

The footprints of most of the burned buildings were also depicted in the resulting animation. This was created using 33cm Maxar Imagery from 12th August (see **3.2.3**). To do this, the burned area containing buildings was manually digitized, and then the building footprints were clipped by this. The extracted buildings were further refined to remove false positives and add any missing ones.

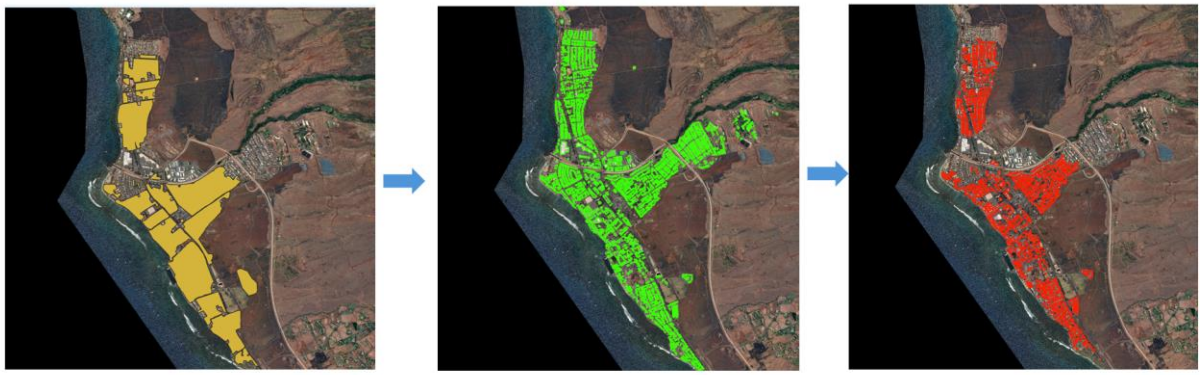

Figure 14 *Burned areas manually digitized(left), All buildings in the dataset(middle), Burned/Destroyed Buildings extracted by Burned area extent(right)*

4.2.4 Burned Zones and Historical Monuments Destroyed

To showcase the areas and landmarks affected in the aftermath of the fire, they had to be digitized. This was done and exported as KML using the online platform Google My Maps.

5 3D MODELLING AND ANIMATION WORKFLOW

This section discusses the steps taken in creating the 3D scene for the animations. Firstly, the Maui Island Fire animation is discussed in detail covering aspects such as the ingestion of terrain and texture files, the ingestion, styling, and animation of fire hotspots, creation of background elements. Also, the camera and lighting setup and subsequent animation will be captured. This is also repeated for the Lahaina Fire and Smoke animation. Issues encountered along the way are also discussed. Lastly, the rendering process is highlighted.

5.1 Maui Island Fire Animation

The Maui Island modelling was largely inspired by tutorials and the work of Peter Atwood was referenced. The Active fire spots and smoke styling are modified versions of his tutorials and files used in creating his Canada Wildfires project.

5.1.1 Modelling procedure

Creating the Terrain Background

To serve as a good contrast to the fire spots, a plain cut to the dimension of the Maui Island boundary is imported into Blender as a shapefile using the BlenderGIS plugin. The CRS for this project NAD83 (PA11)/UTMZone4N, is the appropriate local projection for Maui. This is set as the Scene georeferencing, and all spatial datasets used are in this format. The 10m DEM is also imported and set as a displacement texture for the plain. Upon doing this, 3 modifiers are added to the plain object. A subdivision and a displace modifier. In the subdivision modifier, the values in the “Levels Viewport” and “Render” are changed in the subdivision modifier to 11 to increase the resolution. The process above is repeated for the satellite image (color) background texture.

To account for the resulting displacement on the map edge, a larger satellite image background is used to hide this in the colored version, while a simple plain is created in Blender and styled to hide the plain version.

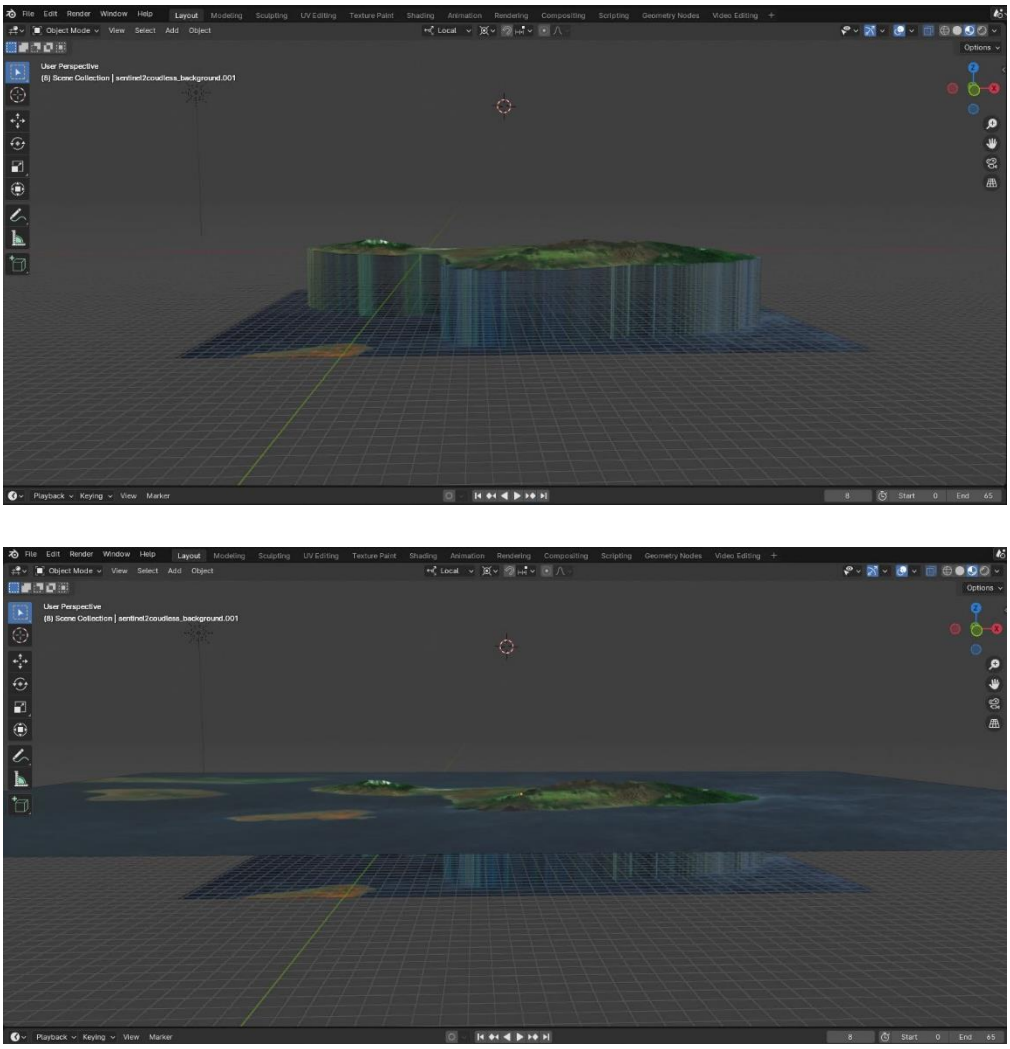

Figure 15 *Colored terrain with (bottom) and without (top) the overlay background.*

Active Fire Spots

For the active hotspots, the Geometry nodes interface is used. Blender's Geometry Nodes system allows users to create complex procedural models by manipulating data attributes. It offers a flexible, node-based approach to modeling, enabling users to design and animate intricate structures with precision and efficiency (Blender, n.d.-b). To ingest the fire points (as converted to CSV with frames added), a simple python script is used in the scripting tab.

To animate the fire spots, a geometry node modifier is added, and the attributes that will be used as geometry input values are selected from the ingested spreadsheet.

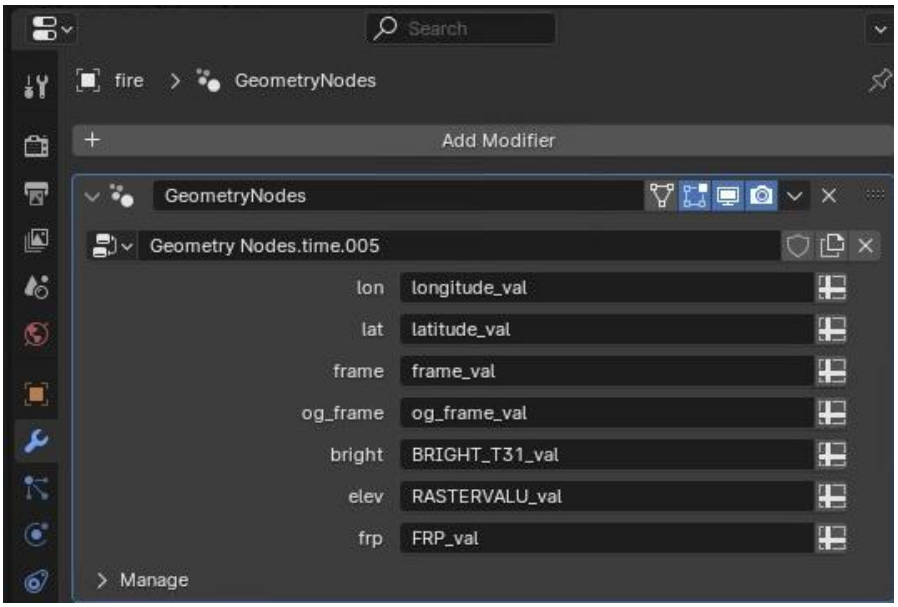

Figure 16 *Attributes used to animate points as ingested in Geometry Nodes*

Geometry Node setup

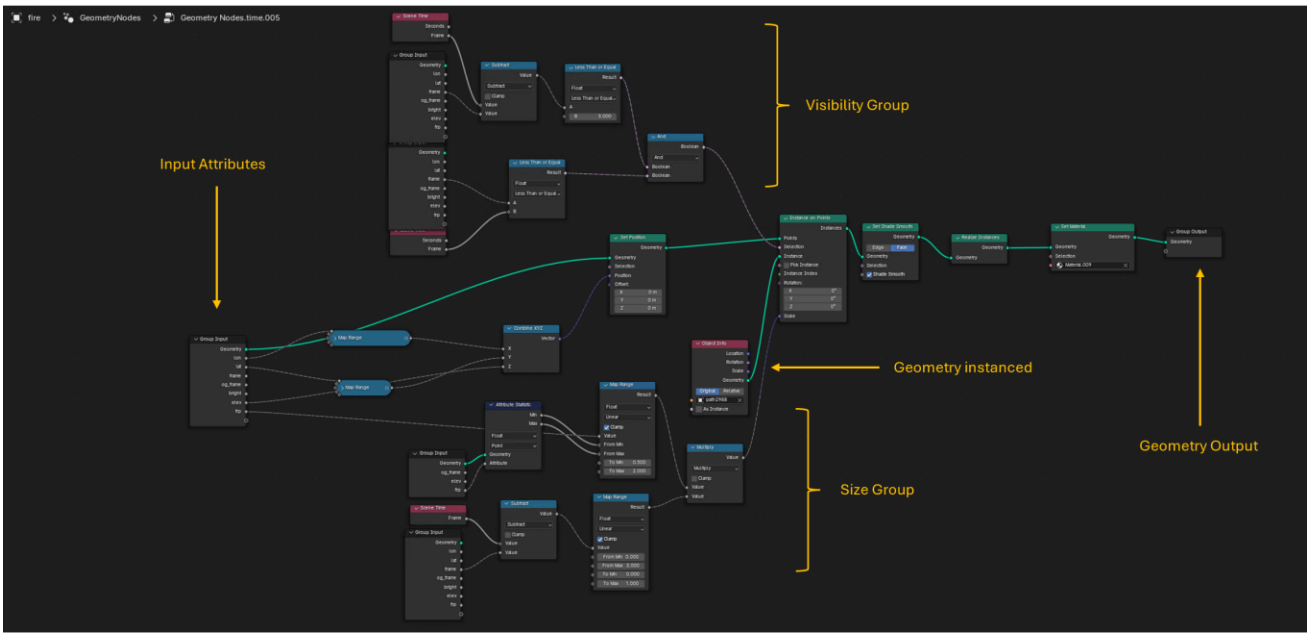

Figure 17 *The Geometry Node setup for the Active Fire Spots*

Primary

The Group Input represents our imported table of points. Importing the fire spots as .csv and working with it in Geometry Nodes ensures that the attributes (frame, FRP e.t.c.), can be leveraged.

Firstly, the position of each point is set by using the *Combine XYZ and Set Position* nodes. The *Map Range* nodes are used to convert the coordinate values from the geographic coordinate range to the projected coordinate range. Then the vertex created is turned into an actual geometry using the Instance to Points node. The geometry used as the instance (*Geometry instanced*) is a simple plain mesh manually created. A Set Shade Smooth node is used to smoothen the instanced geometry (more important for a 3d mesh object than a plane). *Realize instances* work to turn the instanced geometry into an actual geometry. *Set Material* adds a predefined material to the geometry. The final output, as displayed in the viewport, after all the changes have been applied by the geometry nodes modifier is the Group Output.

Visibility Group

The points that are displayed at each frame are controlled here. To ensure that only the points, whose frame is the same as the current frame in the animation, are displayed, a *Compare* node (Less Than or Equal to), is set between the frame attribute of the table and the frame value of the *Scene Time* node. A further step was taken to ensure that each point disappears after a few frames (in this case 3 frames = 1 second). A math (Subtract) node was set between another Group input frame attribute and *Scene time* frame value (this gives the age of the point). Another *Compare* (Less Than or Equal to) node is then added to compare the resulting value to 3 (number of frames). Finally, both values are plugged into a *Compare* (And) node and further into the selection value of the *Instance on Points* node, to ensure that only points whose frame value is less than or equal to the current frame value are displayed, and they will only be visible for 3 frames before they disappear.

Size Group

The size of the fire spots as displayed is modified here. The FRP is used to size the points, The ultimate size of each point is representative of the FRP value which is set to range from 0.5m to 2m (using the *Group Input*, *Attribute Statistics,* and *Map Range nodes*). The Fire Radiative Power(Wooster et al., 2005), which is a measure of the rate of radiant heat output from a fire is used as a proxy for fire intensity. The final size is not instanced at once but grows over 3 frames/1 second. (using the *Scene Time/Group Input*, *Math* (Subtract), and *Map Range* nodes).

Active Fire Material Setup

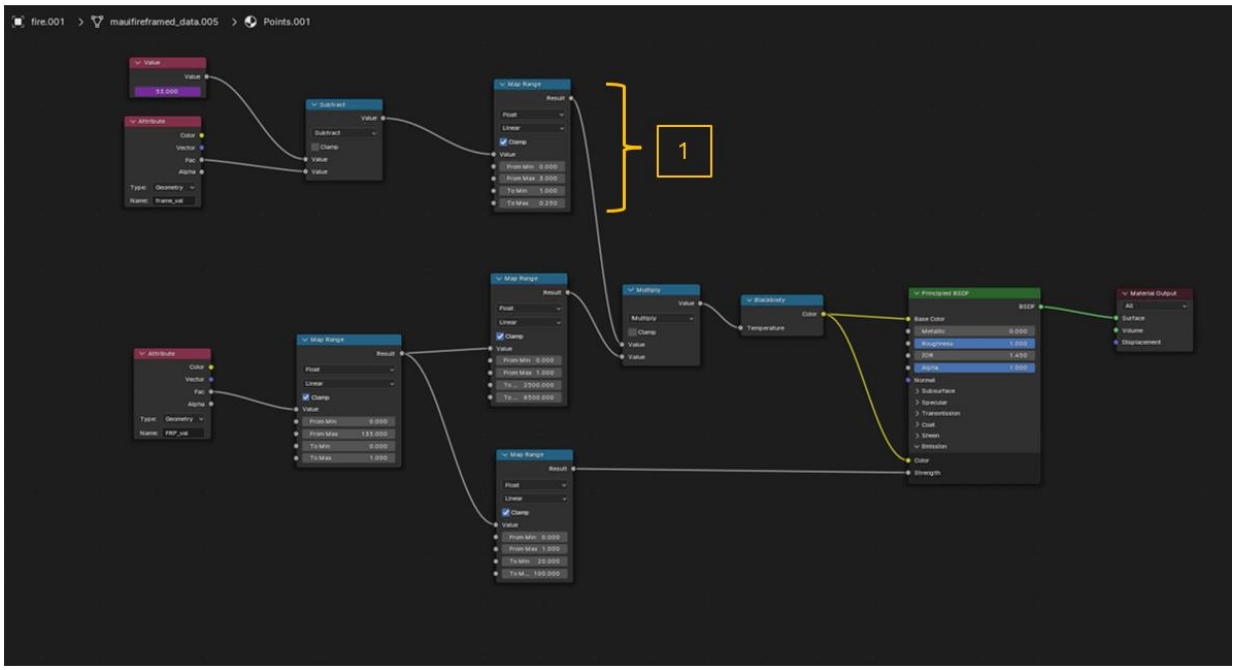

Figure 18 *The material setup as used for the active fire spots*

Similar to the visibility and display above, the material is created also using the FRP as a factor. It is shaded such that the fire intensity grows over 3 frames reaching its final intensity at the third frame. This is achieved by the *Value*(Scene frame)/*Attribute*(frame), *Subtract*, and *Map Range* node group (1).

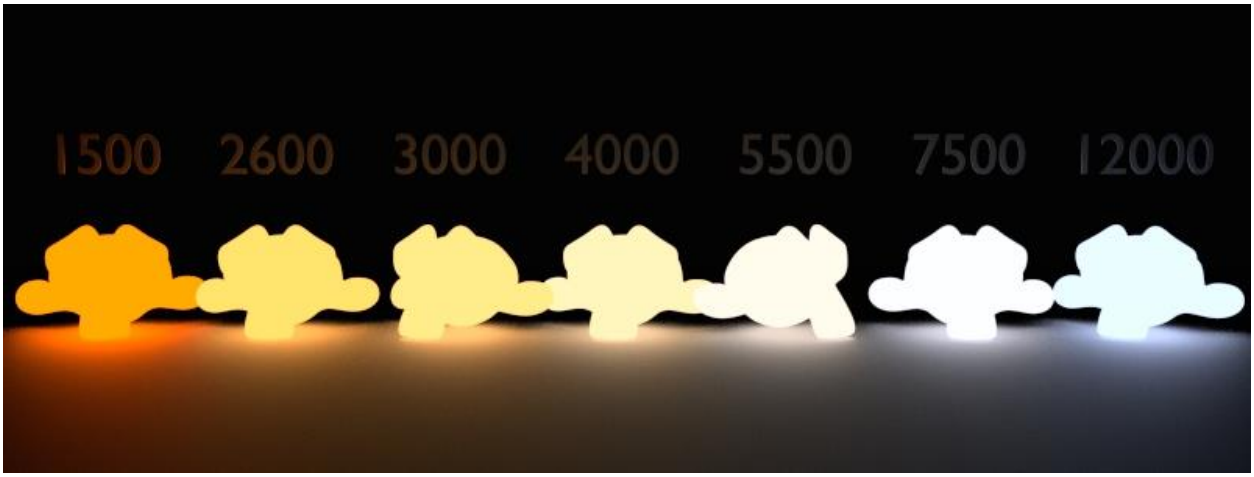

Figure 19 *Color ranges of Blackbody Node* (Blender, n.d.-a)

To increase the brightness of the points based on the FRP value, the FRP value is mapped (*Map Range* node) to a value range between 2500 and 8500 which is then multiplied by the result from the group above to serve as the temperature value of a *Blackbody* intensity node. The *Blackbody* node converts a blackbody temperature to an RGB value. This is used for materials that emit light at naturally occurring frequencies. This node is then plugged into the Base and Emission color of the Principled BSDF. Lastly, the FRP value is mapped once more to a value range between 20 and 100 to serve as the Emission Strength. This setup is illustrated in figure 19.

Transforming Fire Radiative Power (FRP) to color information.

0 – 135 = 2,500 to 8,500

To remap the range of values from [0,135] to [2500,8500], the linear transformation formula was used:

$$y = m \cdot x + c$$

where:

- x is the value in the original range [0,135]
- y is the value in the target range [2500,8500]
- m is the slope of the line,
- c is the intercept.

First, the slope m and intercept c were determined as follows:

The slope m can be calculated as:

$$m = \frac{y_2 - y_1}{x_2 - x_1} = \frac{8500 - 2500}{135 - 0} = \frac{6000}{135}$$

The intercept c is the value of y when x=0 which is 2500.

So, the transformation formula becomes:

$$y = \frac{6000}{135} \cdot x + 2500$$

Afterwards, the x values that correspond to y=2500, 3500, 4500, 5500, 6500, 7500, and 8500 are calculated as follows.

Solving for x in each case:

$$x = \frac{y-2500}{\frac{6000}{135}}$$

Therefore:

For y = 2500

$$x = \frac{2500-2500}{\frac{6000}{135}} = \frac{0}{\frac{6000}{135}} = 0$$

Replicated for all other values of y (2500, 3500, 4500, 5500, 6500, 7500, 8500), x values are 0, 22.5, 45, 67.5, 90, 112.5 and 135 respectively. This was used to create the legend, as depicted in the animation.

Alternative Active Fire Material

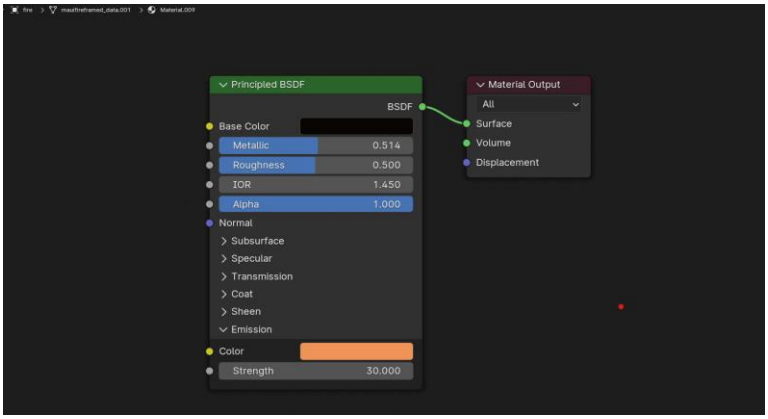

Figure 20 *Material Shader for a simpler alternative shader*

An alternative material for the active fire spots that was created for this work involved using the emissions node of a simple Principled BSDF with bloom effect activated (in Render properties if ENVEE render engine is used), or Glare node in Compositing (if Cycles Render Engine is used). The shader node setup for this is illustrated in Figure 20. Figure 21 is a gif showing what the animation looks like using this setup.

Figure 21 *Animation using the alternative active fire material*

Smoke Modelling Workflow.

If an appropriate smoke resolution had been downloaded, the workflow for ingesting it and using it in Blender would have been as follows:

Firstly, the image maps for each time step downloaded would be converted into an image with a black and white color ramp, such that higher values of AOD are white. A sphere mesh would be created in Blender to represent the sky onto which the image would be applied as a shader. A possible shader node setup to achieve this is illustrated in figure 22.

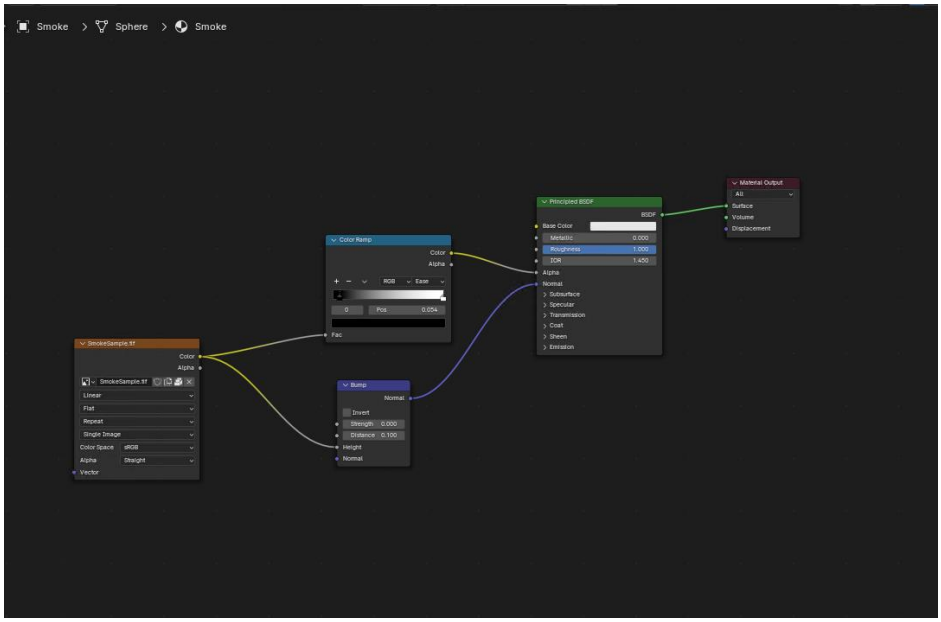

Figure 22 *Possible Smoke Material Shader setup (Atwood, 2024)*

Burned Area

The active fire point was duplicated to create this, such that the same geometry is used. The burn area is animated with the same procedure as the fire points; however, the points do not disappear after a few seconds. The final color change to highlight the areas burned is an unanimated version of the fire points object. Its material is animated to start transparent, and it covers the final 9 frames of the animation.

Other Environment elements

Lighting is created as a sun lamp which is its strength an angle are animated to mimic a sunrise in the initial part of the animation (First 15 frames). Table 9 depicts the lighting animation workflow. The camera is also set to capture the entire island.

5.1.2 Animation Procedure

Animating in Blender involves setting keyframes on elements to be animated. Table 9 illustrates the animation procedure for the light (sun). Keyframes are inserted on the value to be animated at the desired frame. Table 10 illustrates how the elements where animated in this scene.

Frame	Strength	Angle
3	1	0
6	5	10
9	10	15
12	15	20
15	15	45

Table 9 *Sun lamp animation parameters*

Frame	Animated Elements
3 - 15	sunrise, color background
16 - 54	Plain background, Active fire, Burned area
55 - 63	Burned area

Table 10 *Animated elements and their corresponding frame.*

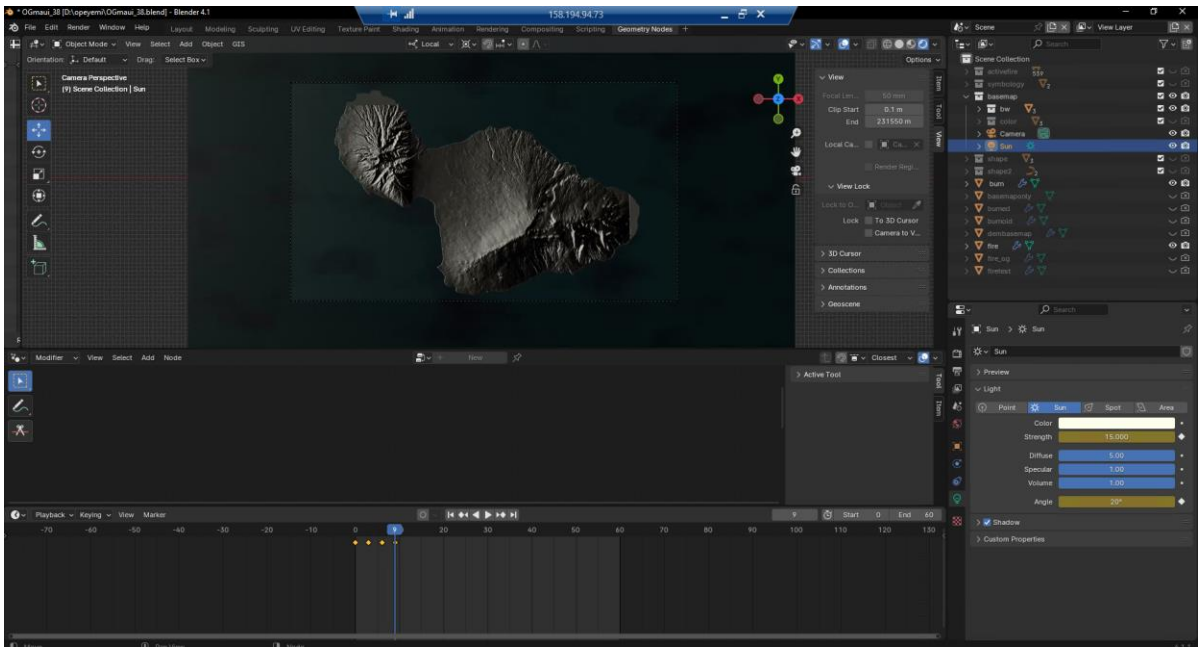

Figure 23 *Keyframes set on the sun lamp for the scene*

5.1.3 Rendering

It is important to reiterate that for this section, a frame rate of 3FPS is used because of the limited time steps available, as expressed in subchapter 3.2.1 of this study. Therefore 3 frames represent 1 second of the animation. Figure 24 illustrates the render settings used for this scene.

Figure 24 *Render parameters for the Maui Fire Animation*

It is generally advised to render into image format (preferably TIF or PNG) instead of video so that if rendering is interrupted, one has the already rendered frames and can just continue from where it stopped. Also, for the purpose of post-processing, the quality of the renders is preserved if they are ingested into Adobe Premiere Pro as an image sequence.

Initial rendering took approximately 1 hour. If the second fire material was used, there is the need to add the glare effect in compositing after the rendering has been done. This image sequence was then taken to Adobe Premier pro for post-processing.

5.2 Lahaina Fire and Smoke Animation

5.2.1 Modelling procedure

3D tiles

Firstly, The Google Photorealistic 3D tiles are downloaded as described above. To facilitate the efficiency of viewport manipulation, the model is scaled down to 10% of its original size. Necessary alignment on the X, Y, and Z axis was done to ensure a seamless transition between the tiles. Figure 25 illustrates the tiles before and after alignment. The 3D tiles come with several default materials without a principled shader. Therefore, lighting and world (background) settings do not affect it. However, the material can be replaced. One of the default materials was edited to introduce a principled BSDF shader and some changes that allow for the desired light and shadow effects to be applied. The material of all the downloaded tiles was then replaced by this edited material. Figure 26 illustrates the edited material node tree.

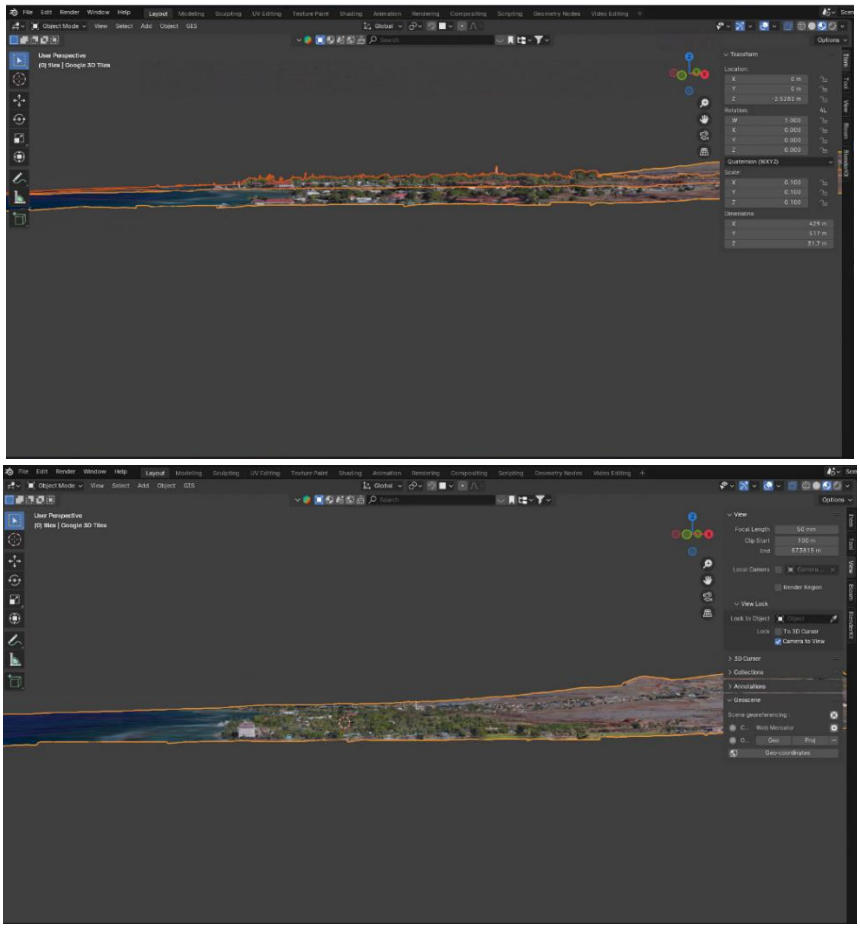

Figure 25 *Tiles before and after alignment.*

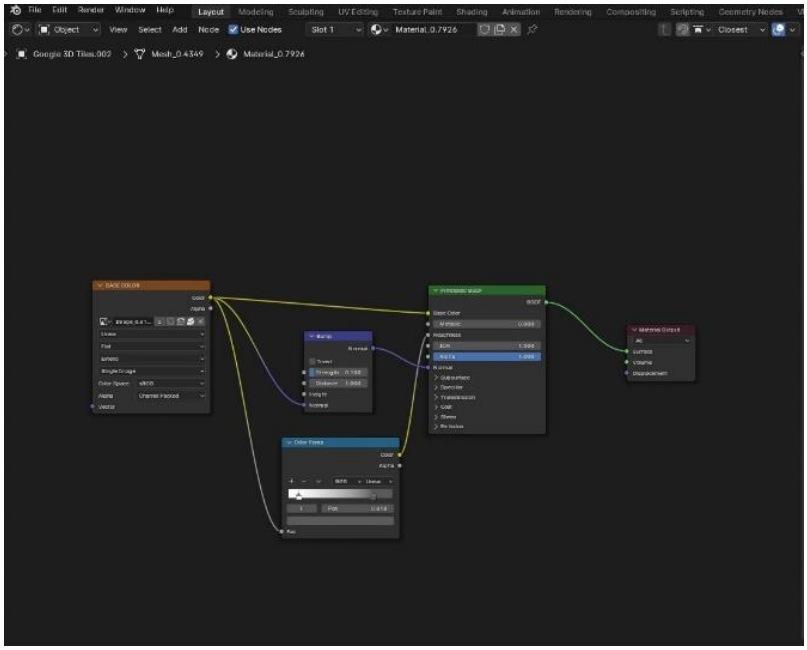

Figure 26 *The material used to replace the default tiles material to ensure the effect of light.*

Fire and Smoke

Blender, being an advanced modeling tool, has numerous capabilities for modeling fire and smoke. One easy iteration is the Quick Smoke effect. (objects - quick effects - quick smoke), as illustrated in figure 27. Such methods of fluid simulations, while more realistic and modifiable, are highly resource-intensive. The use of fluid simulation for a scene as big and dynamic as this would have been unjustifiable.

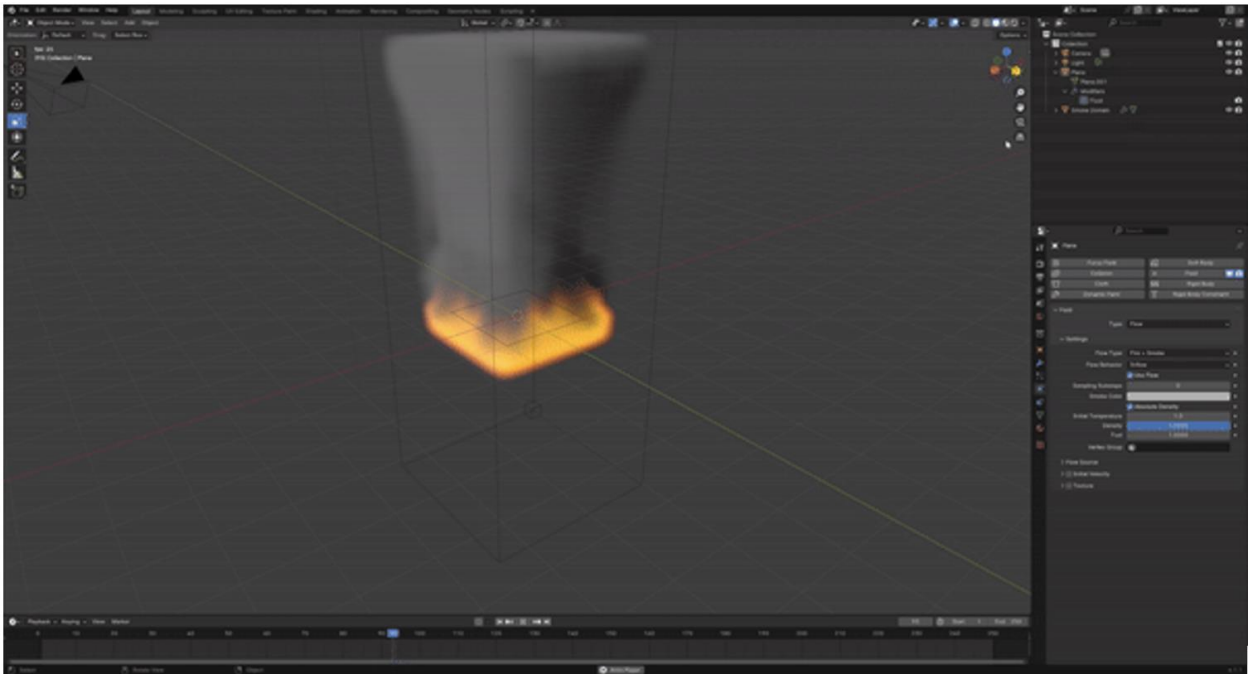

Figure 27 *Quick Smoke effect simulation in Blender.*

However, this study uses another approach, The draw fire tool (Kenan Proffitt, 2023) created by Kennan Profit (Profit, 2024). In the spirit of modeling ease and conserving resources by sacrificing a little flexibility, this tool was used to instance fire and smoke across the scene. Many such tools and plugins are available for various functions in Blender, and indeed are an invaluable source for Blender users. This tool was created as a geometry nodes modifier which modifies a Bezier curve geometry and instances a dynamic fire or smoke material at the vertices along the curve. To use it, a user simply draws a Bezier curve object to which the fire tool has been added as a modifier. Parameters that can be adjusted include the scale (intensity) of the fire, whether one requires just fire, just smoke, or both among others, the rotation and dimensions of the fire. For more information on the tool see (link), and to find out about the creation of the fire material, see (link) For this work, only fire/smoke, and scale options were manipulated and animated.

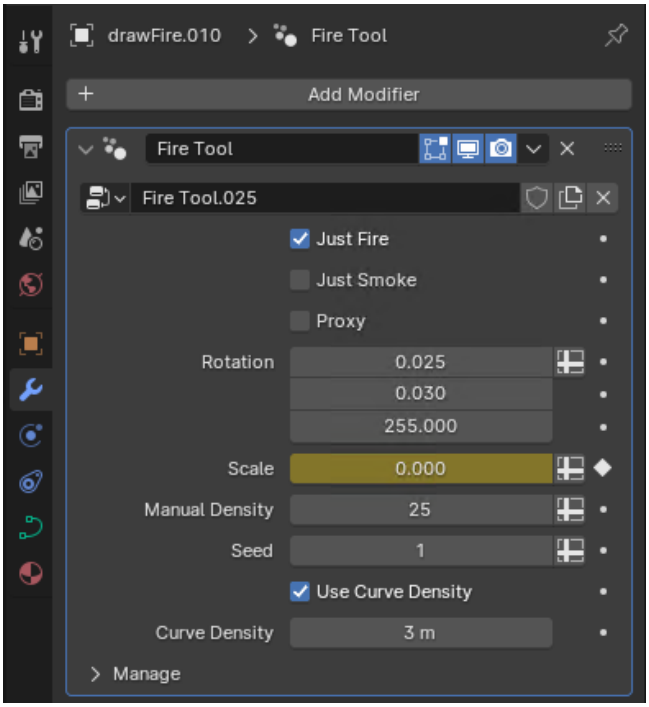

Figure 29 *The modifiers tab of a smoke object showing the Fire Tool. For this work, only the scale factor is animated to show the growth and progression of the fire.*

Figure 30 *Fire material from the Fire tool tested on a section of Lahaina*

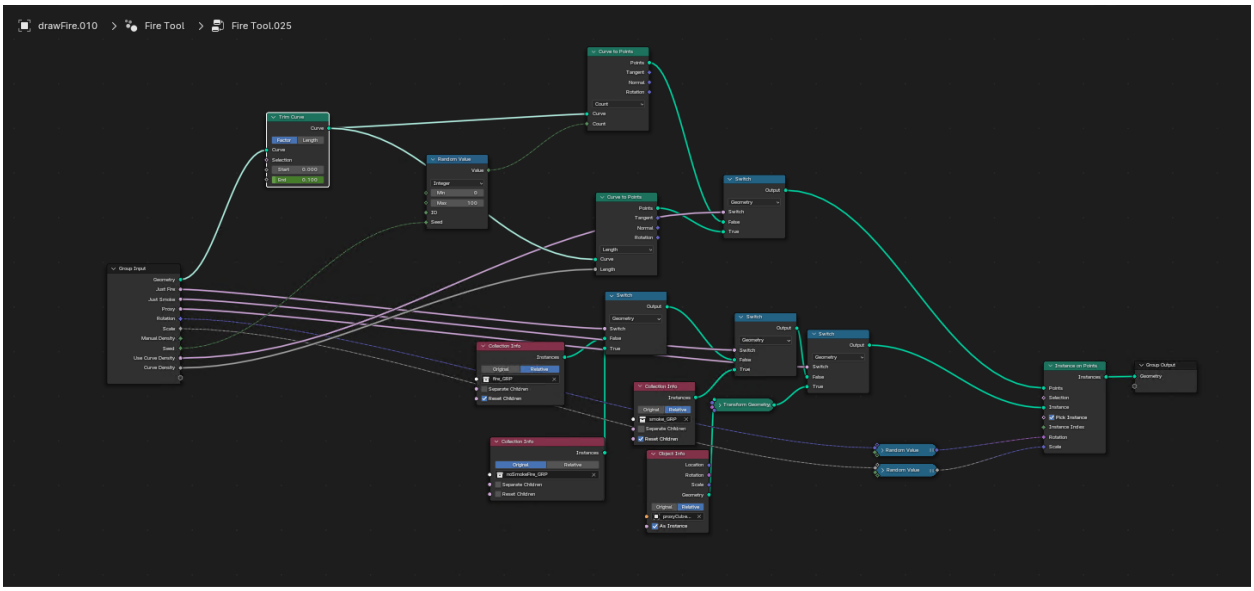

Figure 31 *Fire Tool node tree showing animated Trim Curve modification.*

For this scene, a Bezier curve object was created to which the tool was added as a modifier. This was then duplicated to represent the different sections of the fire (which will be animated to show the progression of the fire). Note that when duplicating, the geometry node tree must be made by a single user. This is important so that each tool is specific to its own object.

Each fire object is drawn in sections as illustrated in figure 32. Each fire object is then duplicated to represent its corresponding smoke object. For the fire object, “just fire” is selected in the fire tool, while “just smoke” is selected for the smoke objects. Lastly, the default fire tool node tree was manually modified to include a *Trim Curve* node, which was animated to allow a gradual growth of the curve in each object rather than an abrupt instance. This was however disabled for some closeup renders.

Factors considered when drawing the fire Bezier curve;

- Make sure to avoid major roads which cannot burn
- Drawing according to the direction of the fire spread to activate the trim curve node.
- Make sure to draw fires in built areas separate from vegetated/grassy areas, as burning spreads and dissipates faster in vegetation than among buildings.

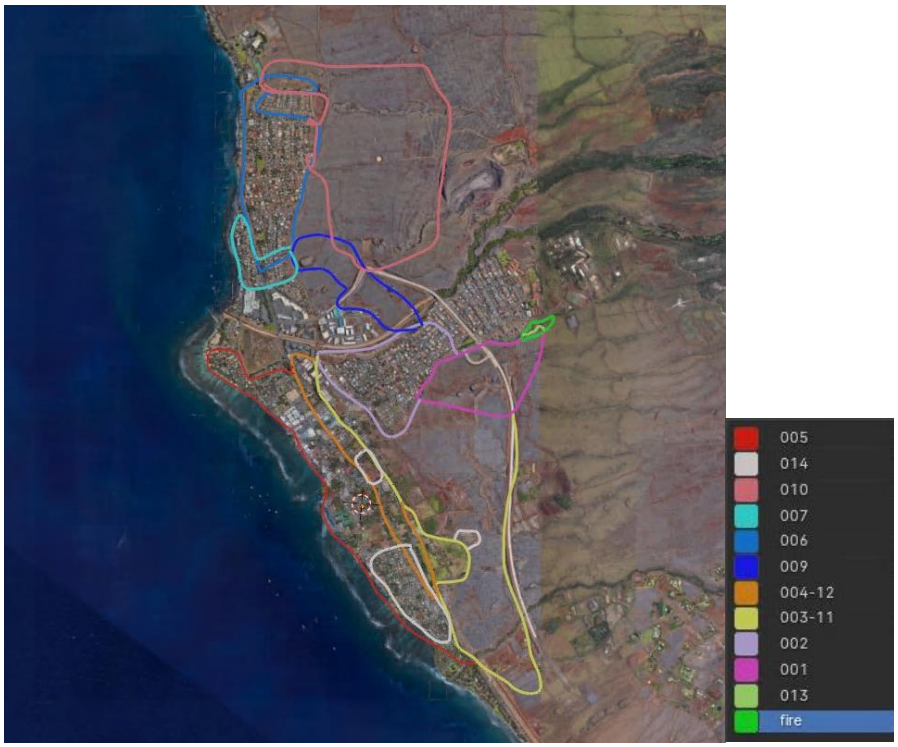

Figure 32 *Sections of the fire and smoke as drawn and animated.*

Atmosphere

The smoke atmosphere was achieved by adding a cube to the scene scaled up to cover the entire scene. A Principled Volume shader was added and textured to give a patchy material to the cube. The mix shader fac is animated so that the material is invisible in the beginning and increases progressively as the fire intensifies. Also to introduce a variability in the noise texture pattern, different positions in the color ramp are animated.

The node setup is pictured in figure 33.

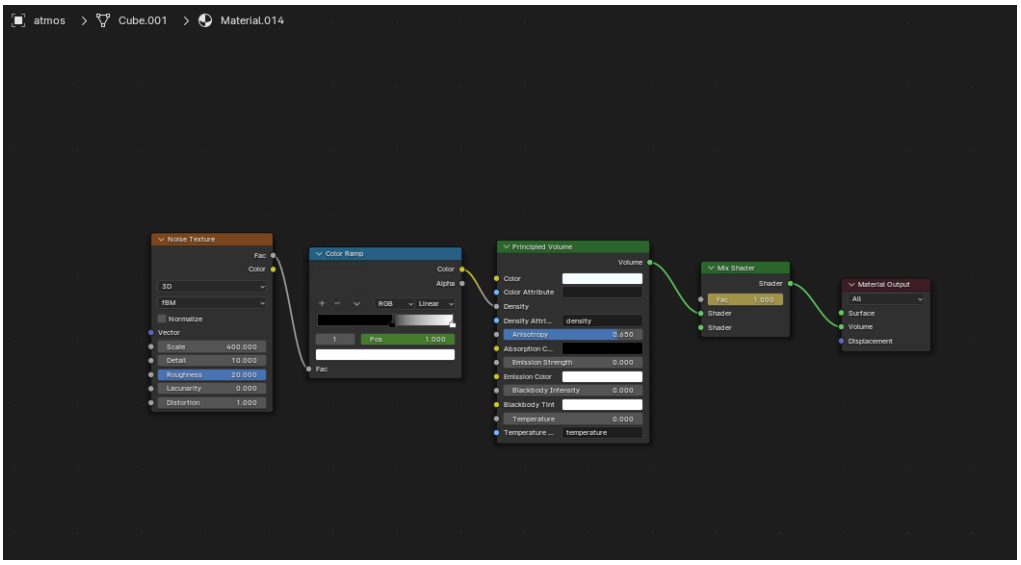

Figure 33 *Atmosphere material setup*

Background

A Clear Sky HDRI was set as the color used for the world settings (Haven, n.d.).

Lighting

A sky lamp was added to the scene. The Background HDR and sun are animated for day and night. Table 11 illustrates the animation process for these elements.

Frame	Time	Date	Time of Day	Sun Lamp		World HDRI
				Strength	Angle	Strength
0	06:30	August 8th	Day	5	45	1
1500	07:00	August 8th	Sunset	2	30	0.5
1860	22:00	August 8th	Night	1	30	0.1
2820	07:00	August 9th	Sunrise	3	30	0.8
3540	11:30	August 9th	Day	5	45	1

Table 11 *Sun Lamp Animation for this scene*

Camera

Separate cameras were set up for the different view angles, after which the view from each camera was rendered separately as listed in the **render** section below.

5.2.2 Animation Procedure

The animation was done based on the timeline identified above. The fire and smoke were animated such that it depicted the natural progression of a fire. By manually creating the fire and smoke scenarios, ensuring to stay true to the verified real-time accounts as reported and what was observable through remote sensing products used, the resulting animation contains a true account of the likely progression of the Lahaina Fires starting from approximately 06:27 August 8th, 2023 (beginning of the brush fire) to 11:20 August 9th, 2023 (Maxar Satellite Image).

Assumptions when animating the fire and smoke

Because there was no true reference for every moment of the entire progression of the fire, the following assumptions had to be made about this section in the workflow, as follows.

- 2 frames represent 1 minute. Therefore, 1 hour corresponds to 120 frames.
- Smoke starts before the fire and ends after it. Therefore, the smoke object for each fire starts/ends between 30 and 200 frames before/after it.
- Fires that start first end first, except otherwise observed in sources.
- Fire and smoke from burning buildings have a higher scale/intensity and burn longer than vegetation. This is because most of the vegetation burnt are grasslike shrubs averaging between 0.5m and 3.5m in height. Therefore, the scale/intensity of fires in the built-up areas ranged from 1 to 2.5, while vegetation fires ranged from 0.5 to 1.5 as illustrated in table 12.

Selective Rendering to optimize efficiency

To save rendering resources and time, it is generally advised to only render what is visible in each frame. Therefore, fire/smoke objects that have not started or have stopped were turned off in render. All Objects (except the first) start disabled in the render and are only turned on when they are actively burning. Therefore, each fire/smoke object was animated to have a Prestart, Start, Peak, Decline, and Stop.

Prestart: The object is turned on in render.

Start: This marks the beginning of the fire. The scale of the fire is increased to at least 1.

Peak: At this frame, the fire or smoke is at its peak intensity

Decline: The scale of the fire is reduced to show it dying out

End: The scale is turned down, and the object is turned off in Render.

Fire Objects

Object Name	Prestart	Start/Scale	Peak/Scale	Decline/Scale	End/Scale
fire	0	300/1	500/1.5	900/1	1200/0
fire .001	1019	1020/1	1100/1.5	1500/0.5	1800/0
fire.002	1090	1100/1	1200/2.5	1800/1.5	2500/0.5
fire.003	1190	1200/1	1500/1.5	1900/0.5	2200/0
fire.004	1290	1300/1	1400/2.5	1800/1.5	2700/0.5
fire.005	1300	1320/1	1420/2.5	2100/1.5	2700/0.5
fire.006	1700	1720/1	1920/2.5	3000/2	3500/0.5
fire.007	1700	1720/1	1920/2.5	2900/2	3200/0.5
fire.009	1590	1600/1	1700/1.5	1900/0.5	2400/0
fire.010	2000	2020/1	2200/1.5	3000/1	3600/0.1
fire.011	1190	1200/1	1500/1.5	1900/0.5	2200/0
fire.012	1290	1300/1	1400/2.5	1800/1.5	2700/0.5
fire.013	900	970/1	1020/1.5	1200/1	1300/0
Fire.014	1300	1320/1	1420/2.5	1920/2.5	2700/0.5

Table 12 *Frames at which fire objects are animated and the corresponding scale*

Corresponding Smoke Objects

Due to the nature of the smoke material in the fire tool, the scale needed to be larger than the fire objects. Therefore, the scale for smoke objects ranged from 2 to 4 in built-up areas and 1 to 3 in vegetation.

Object Name	Prestart	Start/Scale	Peak/Scale	Decline/Scale	End
smoke	0/0	150/3	300/2	900/1	1400/0
smoke .001	1009/0	1010/3	1080/3	1500/2	2000/0
smoke.002	1000/0	1100/4	1200/3	1800/3	2700/1
smoke.003	1170/0	1200/3	1500/3	1900/2	2500/1
smoke.004	1200/0	1270/4	1400/3	1800/3	2800/1
smoke.005	1270/0	1300/4	1420/3	1800/3	2200/1
smoke.006	1600/0	1680/4	2820/3	3000/3	3500/1
smoke.007	1600/0	1680/4	2500/3	2900/3	3200/1
smoke.009	1500/0	1570/3	1700/3	1900/2	2600/1
smoke.010	1900/0	1980/3	2200/2	3000/2	3600/2
smoke.011	1170/0	1200/3	1500/3	1900/2	2500/1
smoke.012	1200/0	1270/4	1400/3	1800/3	2800/1
smoke.013	900/3	970/3	1020/3	1200/2	1500/0
smoke.014	1270/0	1130/4	1420/3	1920/2	3000/1

Table 13 *Frames at which smoke objects are animated and the corresponding scale.*

5.2.2 Rendering

For all camera angles in this scene, render properties are set to Viewport Standard 1920 by 1080, at 30fps. All frames were rendered to *.tiff* format, according to convention.

Table 14 depicts the render details for each render output in the scene. Lahaina Fire (Impact/Historical Landmarks) does not have a corresponding Time/Date duration because it depicts an aftermath scenario.

Name	Duration		Frame range	Frame Count	Render Time
	Date/Time	Output			
Lahaina Fire 2023 (South-western View)	August 8th 06:30 – August 9th 12:34	120 seconds	0 - 3600	3600	40 hours 20 minutes
Lahaina Fire 2023 (Eastern Hillside View)	August 8th 06:30 – August 9th 12:34	120 seconds	0 - 3600	3600	40 hours 20 minutes
Lahaina Fire 2023 (Harbor View)	August 8th 14:50 –23:48	36.6 seconds	1000 - 2100	1100	5 hours 30 seconds
Lahaina Fire (Impact/Historical Landmarks)	-	66.7 seconds	1000 - 3000	2000	1 hour 40 minutes

Table 14 *Render details for each camera angle in the scene*

5.3 Post-processing / Video Editing

The individual files containing the .tiff images were imported into individual Adobe Premiere Pro projects as image sequences. Elements such as Title, Description, Callouts, Time counter Imprint, and Audio were added in this step.

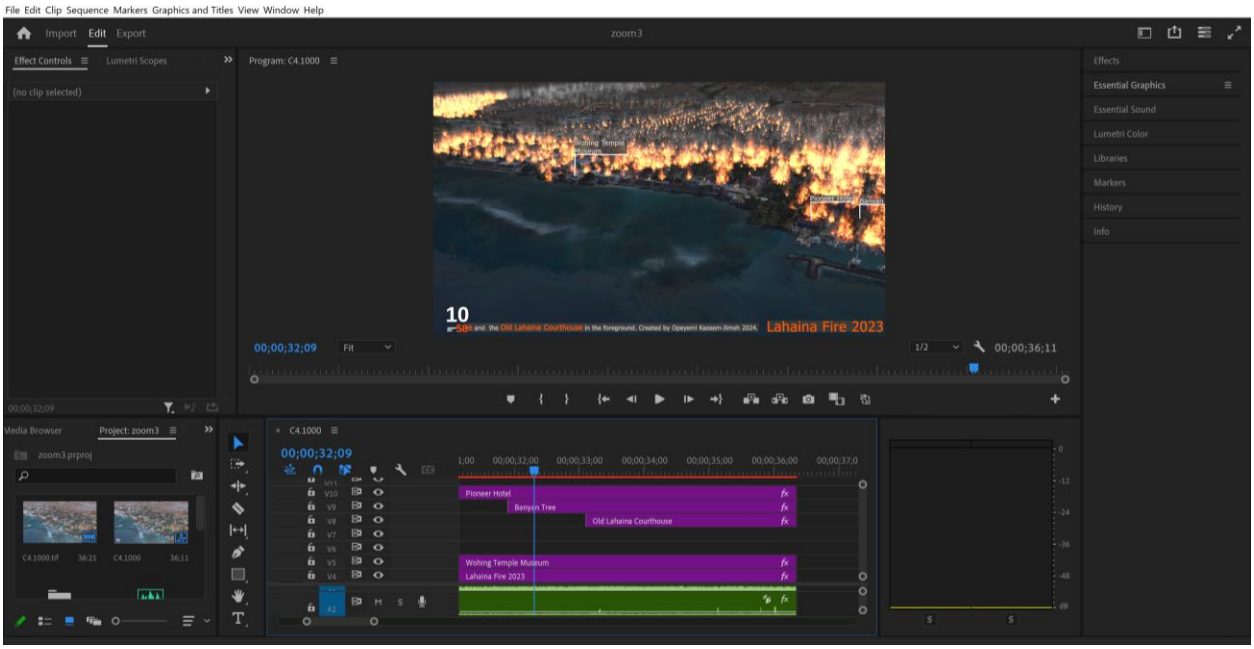

Figure 34 *Adobe Premiere Pro User Interface as adopted in one of the video projects.*

6 RESULTS

This section discusses the outputs from this study. Five separate video animations from separate camera angles were produced to illustrate the progression of the Maui Island and Lahaina Fires of 2023. They are described below.

6.1 Overview Animation of Maui Island Fire

This is the result of the Maui Island Animation. It shows an overview map of the island and visualizes the active fire spots as bright objects animated to appear at the appropriate time stamp and disappear afterward.

The video has 3 sections, the first of which shows the light rise of Maui Island. Here the background is the 10m DEM as terrain, textured with Sentinel 2 cloudless composite data. The title, description, inset map, scalebar, and imprint appear at the beginning and are permanent throughout the video. The animated wind icon is active from the beginning while the active fire points are burning. The second section starts with the transformation of the background to a plain grey textured terrain. This serves as a better backdrop for the active fire spots. As the fire spots appear so do their callouts, and corresponding time stamps. The legend also appears in this section. After the fire spots stop, the burn scars remain and are highlighted in red towards the third section. Finally, line charts showing the impacts (Area burned, Casualties, and Buildings Damaged) are displayed.

Figure 35 shows a still sequence from the animation, while Figure 36 highlights the layout elements.

Figure 35 *Still Sequence from Overview animation of Maui Island Fire active fire data.*

Figure 36 *Animation Layout elements (Video Link)*

6.2 Animation of Lahaina: South-western view Overview Animation of Maui Island Fire

This animation shows the initial 30 hours of the fire. Starting from 06:30 hours on August 8th, 2023, to 12:34 hours on August 9th. The camera looks from the southern coast of the island just beyond where the affected buildings start. This captures the entire burn zone and illustrates the fire in Lahaina starting and progressing.

The title, description, time counter, and imprint start at the beginning and are permanent. As the animation progresses, callouts explain the progress of the fire, the area currently burning and highlight specific landmarks. At specific time steps where verification data is available in the form of video snapshots or satellite data, these are also displayed at the corresponding timestamp. The video stills are gotten from NBC News (NBC News, 2023).

Figure 37 shows a still sequence from this animation, while Figure 38 illustrates its layout elements.

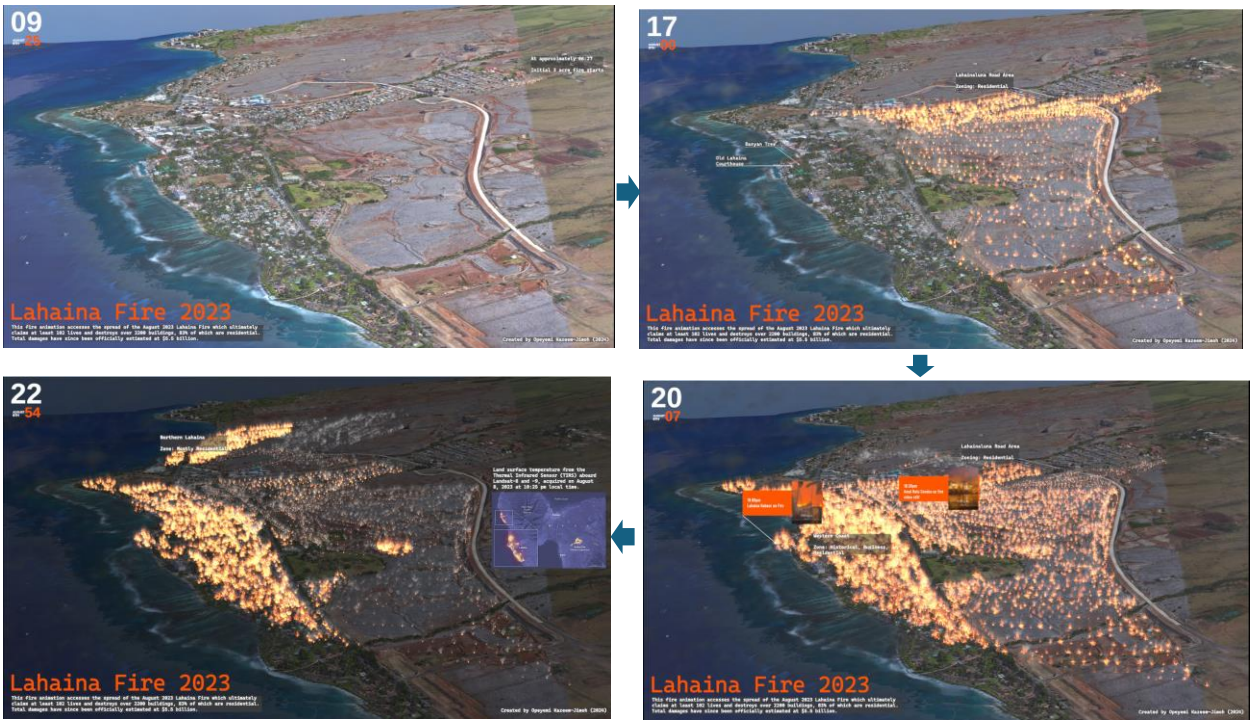

Figure 37 *Still sequence from the animation*

Figure 38 *Animation Layout elements (Video Link)*

6.3 Animation of Lahaina fire: Eastern hillside view Animation of Lahaina: South-western view Overview Animation of Maui Island Fire

This animation also shows the initial 30 hours of the fire. Starting from 06:30 hours on August 8th, 2023, to 12:20 hours on August 9th. The camera looks from the eastern hillside and offers a closer view from the fire ignition point. This view also captures the entire burn zone, albeit with a steady camera movement facing first to the south and then to the north. It shows the same fire progression as in the above animation.

The title, description, time counter, and imprint start at the beginning and are permanent. As the animation progresses, descriptors explain the progress of the fire, and the area currently burning and highlight specific landmarks. The major road and stream in view are also labeled using callouts. The location parameters of the callouts and labels had to be manually animated every few frames because of the dynamic nature of the camera angle. This was a tedious process which resulted in a jittery effect. However, given the short time frame, this could not be significantly finetuned further. Although similar to the previous animation in that it starts at 06:30 hours, unlike that one, this time counter counts in hours and minutes, such that users get an idea of how much time passes as the fire progresses.

Figure 39 shows a still sequence from this animation, while Figure 40 illustrates its layout elements

Figure 39 *Still sequence from the animation*

Figure 40 *Animation Layout elements (Video Link)*

6.4 Animation of Lahaina fire: Harbor View Animation of Lahaina fire: Eastern hillside view Animation of Lahaina: South-western view Overview Animation of Maui Island Fire

The purpose of this animation is to focus more on the historical district on the west coast of Lahaina and how the fire spread there. Starting from 02:50 hours and ending at 23:48 on August 8th, 2023. The camera looks from just above the harbor and zooms in and centers on the Banyan Tree and the Old Lahaina Courthouse at the heart of the historical district. The view then shifts first to the left (towards the south), then to the west (towards the north) to see the fire burning landmarks like 505 Front Street Shopping Mall and Wohing Temple Museum. It shows the same fire progression as in the above animations. The timer gives a view into when this likely occurred in real time.

The title and time counter start at the beginning and are permanent. The description is animated as "*text crawl"*, such that it scrolls across the bottom of the screen as the video progresses. As the animation progresses, callouts highlight specific landmarks. Similar to the Hillside view animation, the location parameters of the callouts had to be manually animated every few frames because of the dynamic nature of the camera angle. The jittery effect was particularly prominent in this case because the landmarks themselves were mostly covered in flames and were not always within frame with some appearing for only a few seconds. Once more, given the short time frame, this could not be significantly finetuned further.

Figure 41 shows a still sequence from this animation, while Figure 42 illustrates its layout elements.

Figure 41 *Still sequence from the animation*

Figure 42 *Animation Layout elements (Video Link)*

6.5 Lahaina Fire Animation: Aftermath (Damage and Historical Landmarks)

Animation of Lahaina fire: Harbor View Animation of Lahaina fire: Eastern hillside view Animation of Lahaina: South-western view Overview Animation of Maui Island Fire

The purpose of this animation is to show the aftermath of the fire particularly in the historical district of Lahaina which was mostly destroyed. The animation is in 2 sections.

The first section shows a side-by-side view of a fly-through from the extreme southwestern part of the burn zone in Puamana Community. In this section of the flythrough, damaged and undamaged buildings were highlighted using individually colored points. A legend is made available corresponding to the structures that are within view. The title, description, and imprint are permanently displayed. On the right side is the 3D model output of this study, while on the right is drone flight footage of the actual area captured 4 months after the fire in December 2023 made available on YouTube (Jesse G. Wald, 2023). Adequate permission was sought and granted from the creator for the footage to be used in this study. To better align the two separate videos, such that they can be comparably viewed, the Blender render had to be slowed down by 40% while the drone footage had to be sped up to 300%.

The second section of the flythrough starts when footage from YouTube stops. Although there is no longer real-life footage available, the remainder of the flythrough depicts the 3D model of the historical area before the fire as rendered from Blender. The purpose of this section is to showcase the quality and realism of Google's 3D photorealist tiles and to show the eventually damaged historical artifacts like the Honjwanji Mission, The Waiola Church, and prominent structures like the Aina Nalu Condo Complex. In the supporting story map to this study, images of the aftermath of these structures are showcased.

Track points are placed to identify corresponding structures, as represented in the legend. Like the two preceding animations, the location parameters of the points had to be manually animated every few frames because of the dynamic nature of the camera. The jittery effect as discussed above persists but is slightly improved here. Also of note is the fact that the outdated nature of the 3D tiles in some places is evident in the "Same Plot, Different Structure" point. Here, it is observed that a different structure has since been erected on the same plot since Google the 3d scan was done for Google. The lack of transparency in the origin and processes by which Google gets its 3D scans means that this question cannot fully be understood.

Figure 43 shows a still sequence from this animation, while Figure 44 illustrates its layout elements.

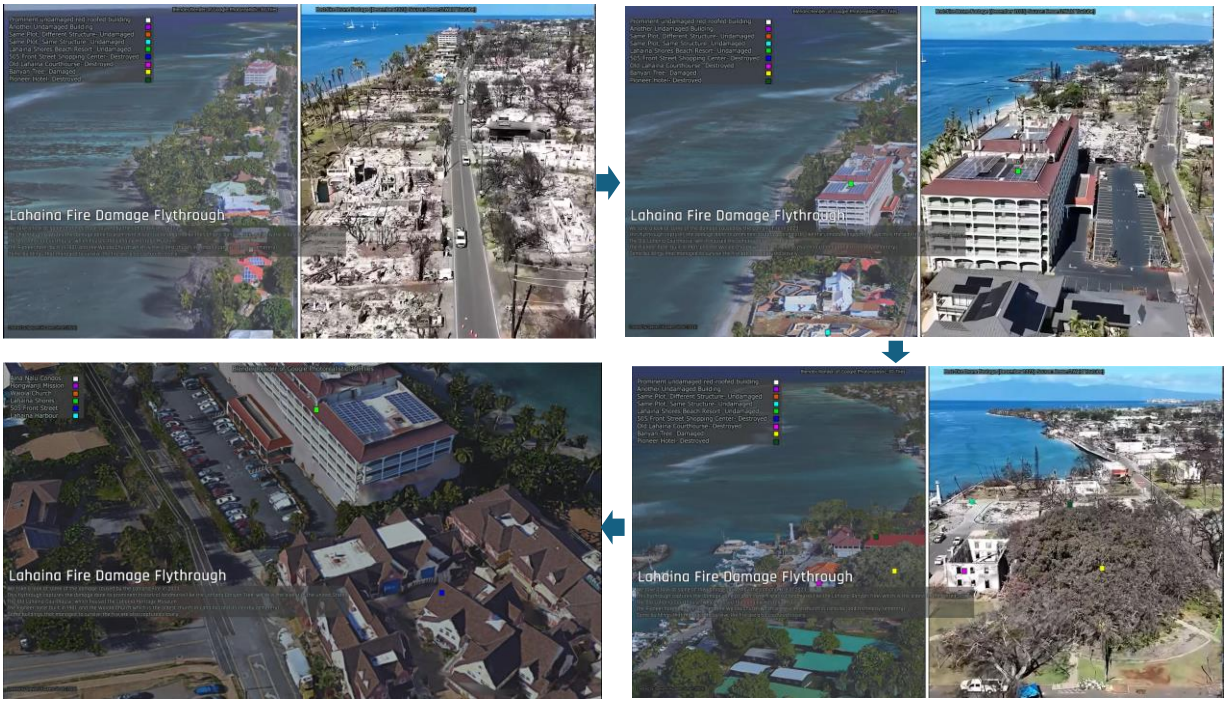

Figure 43 *Still sequence from the animation*

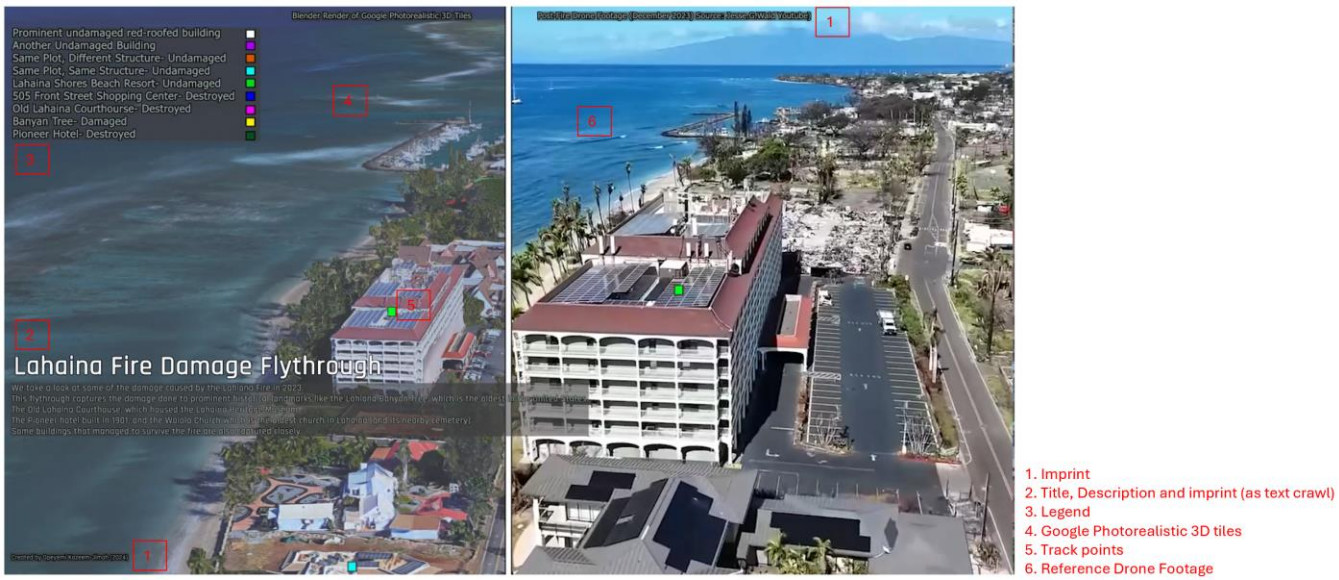

Figure 44 *Animation Layout elements (Video Link)*

7 EVALUATION

This section evaluates the accuracy of this study in modeling the Maui Island Fire of 2023. Here, the resulting 3D animations are assessed based on remote sensing data and the most detailed official timeline so far from the Hawaii Department of the Attorney General(Hawaii DOAG, 2024).

7.1 NASA Thermal Imagery and Shortwave Infrared

The calculated land surface temperature from the Thermal Infrared Sensor (TIRS) aboard Landsat-8 and -9, acquired on August 8, 2023, at 08:25 UTC (Local time: 10:25 pm (22:35) on August 8, 2023) was used in this evaluation. It is available on NASA's Disaster Mapping Portal (NASA Disaster Portal, 2023). The units for this product are Kelvin (K).

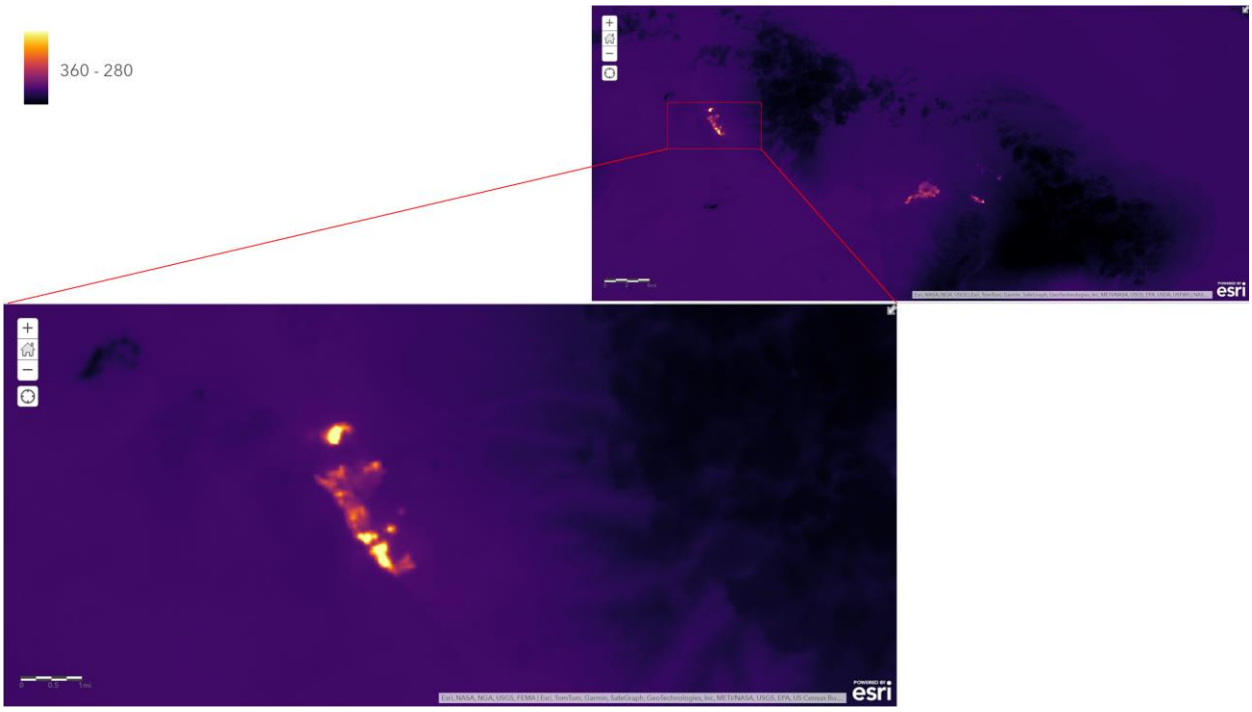

Figure 45 L*and Surface Temperature from Landsat TIRS acquired 10:25 pm (22:35) local time on August 8, 2023 (NASA Disaster Portal, 2023)*

The shortwave infrared imagery of the Maui Island wildfires was also captured by the Operational Land Imager (OLI) on Landsat 8 on Aug. 8, 2023 (time unknown), as seen in Figure 46. Fires are shown in yellow. The shortwave infrared data were overlaid on a natural-color mosaic image based on Landsat 8 observations for added geographic detail. This data source was simultaneously referenced for this evaluation.

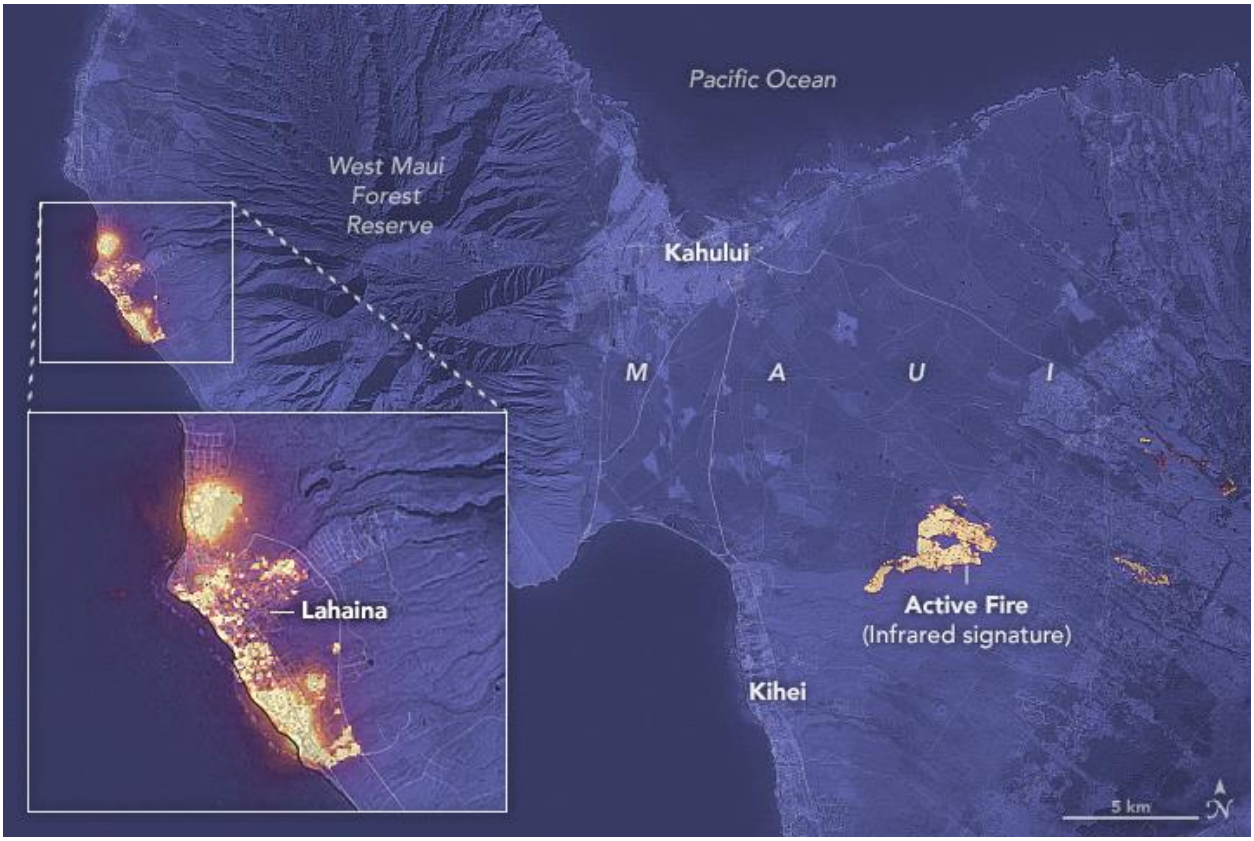

Figure 46 *Earth Observatory image by Lauren Dauphin, using Landsat data from the U.S. Geological Survey.* (NASA Applied Science, 2023)

7.2 Comparison

It is important to note that all forms of remote sensing data carry an element of abstraction, given the scale of the area and the limitation of the sensors and instruments (Lillesand et al., 2015), (Campbell & Wynne, 2011). However, this is the closest to real-time data available for this scenario at this scale, therefore it was deemed suitable. While the acquisition time of the shortwave infrared image is unknown, the fire outline is very similar to the surface temperature data. Therefore, it is assumed that they represent almost exact time and conditions. Taking a still from the animation at the time stamp of the acquisitions, a comparison of the fire progression is made. Figure 47 illustrates this.

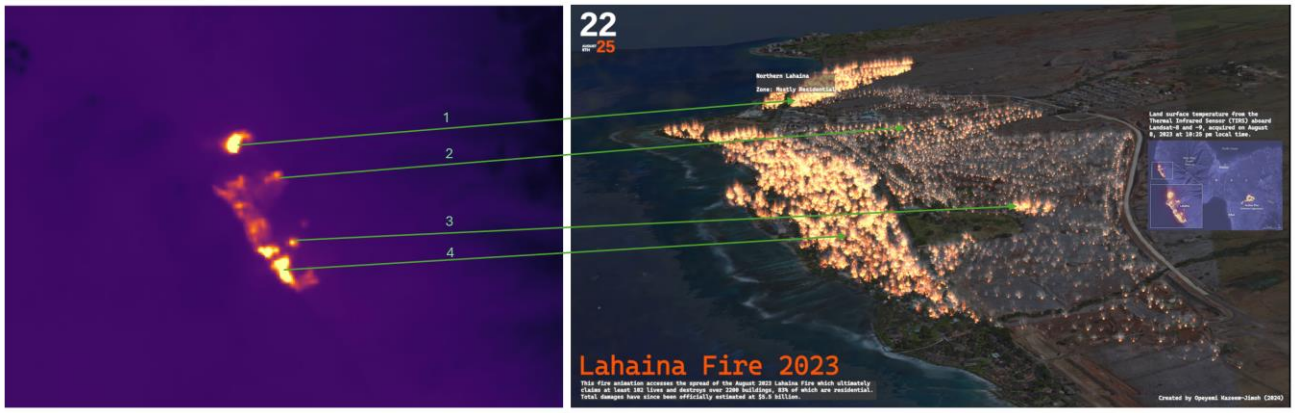

Figure 47 *Landsat TIRS Imagery (left), Still from output animation (right)*

The fire intensity in northern Lahaina residential (1) is visible in the surface temperature data, same as for the Lahainaluna area (2) where the fire had initially intensified and is now waning. 3 shows the still high fire intensity in the apartment complex on Aulike Street while (4) shows most of Puamana Community and Front Street still burning intensively. The depiction of the fire progress at the specified point in time is highly analogous to these data sources.

7.3 Maxar Satellite Imagery

Maxar's publicly available 33cm satellite imagery (as described in section 3.2.4) acquired on August 9th at 11:20 local time was visually compared to evaluate the output of this study. Fire cannot be seen in the satellite imagery, but this is not to say that some parts were not still burning. The ability to see smaller fires at this scale, time of day, and sensor angle is limited. However, since this is an optical imagery that depicts what the human eye can see at 33cm spatial resolution, it was deemed adequate for this evaluation.

Figure 48 *Maxar 33cm Satellite Imagery (left), Still from output animation (right)*

7.4 Comparison

Judging by the smoke position in the agricultural zone to the north of Lahaina (1), we can tell that a fire is still active albeit on a smaller scale, and that the fires in most of the area have since subsided. Given the natural progression of the fire and the fact that in the north, the fire started much later, it is assumed that the fire in the residential part is still burning (2), even though it is not obvious on the satellite image.

7.5 Hawaii Attorney General Progression Timeline.

Hawaii state officials released the Lahaina Fire Comprehensive Timeline Report, which is the first phase of an independent analysis conducted by the Fire Safety Research Institute (FSRI), part of UL Research Institutes. The report chronologically details the major events and response efforts related to the catastrophic fire that struck Lahaina, on August 8–9, 2023. Figure 49 is an animation presenting the findings of this report. It shows the progression of the fire from verified observations made in real time. Comparing this to the resulting animation from this study gives a good overview of the quality of the fire progression modeling done. This data set was not consulted before this evaluation.

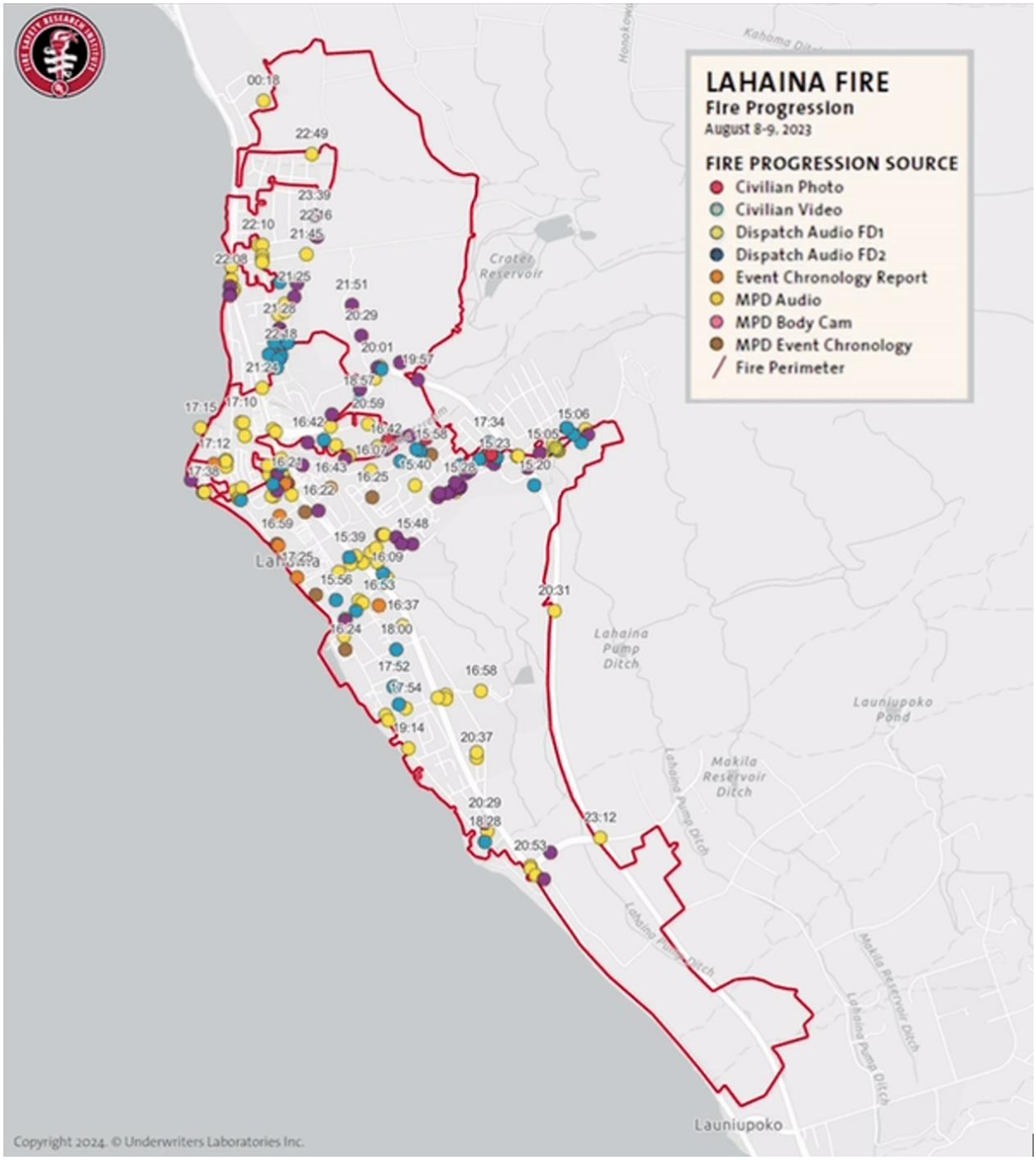

Figure 49 *Fire progression report (Fire Safety Research Institute et al., 2024)*

7.6 Comparison

Figures 50 to 54 show a side-by-side comparison of the Fire Safety Research Institute (FSRI) progression animation to the progression animation done in this study at 5 different time steps, August 8th (15:56, 18:28, 22:18), August 9th (02:51, 06:07). The fire progression exhibits a high degree of similarity across both depictions.

Figure 50 *Fire progression animation by Fire Safety Research Institute et al., 2024 (left), Modelling output of this study (right)*

Figure 51 *Fire progression animation by Fire Safety Research Institute et al., 2024 (left), Modelling output of this study (right)*

Figure 52 *Fire progression animation by Fire Safety Research Institute et al., 2024 (left), Modelling output of this study (right)*

Figure 53 *Fire progression animation by Fire Safety Research Institute et al., 2024 (left), Modelling output of this study (right)*

Figure 54 *Fire progression animation by Fire Safety Research Institute et al., 2024 (left), Modelling output of this study (right)*

In Figure 50, the fire had not progressed as far into the historical center as in the FSRI depiction. While in Figure 51, the fire had expanded very similarly to the FSRI observations. It is also observed that the agricultural area in the south is likely burning at this time step, as depicted in this study's animation and as found in Maxar Satellite Imagery from August 9th, however, there were no specific entries in that location in the FSRI observations. In Figure 52, as in the FSRI animation, the fire has now spread to the north. In Figures 53 and 54, there is still a high correlation between both depictions, Although, as is expected in the natural progression of a fire, the fire in the central and southern areas has now subsided.

8 DISCUSSION

While conducting this study into developing a workflow for the retrospective modeling of a wildfire progression, which resulted in the creation of 5 video outputs, each from different views of the fire progression model, some successes and challenges were identified which will now be discussed.

8.1 Evaluating Google Photorealistic 3D Tiles

Google's Photorealistic 3D tiles (as described in subchapter 3.2.5) are leveraged in this study. It is considered cutting-edge in its availability and quality and saved a significant amount of time in the workflow of this study. Given the lack of an openly available, recently acquired, high-resolution Digital Surface Model (DSM) of Lahaina, in the absence of the Google 3D tiles, a workflow would have been required to create models of the area from scratch. Although there exist city generator plugins for Blender that produce high-quality 3D city models with a few steps, they do not depict real cities. If a real model of Lahaina were to be created, it would have required modeling every building, plant, road, and other environmental features. This would not only have been labor and resource-intensive, but it would also have taken significant time.

However, there are a few challenges with its use as observed below.

- **Data is not up to date:** As highlighted in section 3.2.5 of this study and evidenced in the Damage and Historical Landmarks animation (section 6.5), the 3D tiles are outdated in some areas.
- **Input source and methodology behind its production non-transparent:** Although a few input sources were identified in subchapter 3.2.5, sources of tiles and acquisition times for specific areas are not openly available.
- **It may be costly for larger projects:** Due to the relatively small scale of this study area (7km by 3km), all tiles downloaded used in this study only utilized the 200 free monthly credits, gotten automatically from the creation and use of a standard Google Cloud account, plus $5 worth of credits extra. This may be significantly higher for a larger area as more credits are consumed with each download.
- **Material editing is not flexible:** Unlike individually created 3D models of the environment elements, whose structure and material can be easily manipulated. This is not possible for Google 3D tiles. This is understandable, however, since they are created from 3D scans of the area.

8.2 Active fire data

This was found to be useful only on a small-scale depiction (zoomed out). Upon zooming into the Lahaina area, the fire points were not useful in explaining the fire's progression. This is because each point is the center point of a 375m-by-375m pixel within which fire was detected (NASA-FIRMS, n.d.). It is very limited in showing how the fire progressed on a submeter level as was analysed in this study. However, real-time videos, images, and commentary from social media and news outlets, verifiable through Google Maps and satellite imagery (building locations identified in updated burn Google Maps) were more useful for piecing together a realistic progression of the fire.

8.3 Modelling and Animation

While the background elements such as the terrain and 3D model of the study area are as geographically accurate as can be, the manual effort was made to animate elements like the fire and smoke model as well as the callout/labels.

While the fire/smoke path was manually interpreted from source imagery, it does not describe the exact path that the real fire took. This is because no data source currently exists, that constantly monitors such fires at the right spatial and temporal scale/resolution. Only snapshots in time are available and were leveraged and interpolated to represent a progressive spread of the fire. Therefore, a level of abstraction exists.

The main software used in this study, Blender for modeling and Adobe Premier Pro for Video editing had to be learned from scratch to carry out this study. Therefore, while this was highly time and resource-intensive, requiring significant effort, there is still significant room for improvement. Given more time, this author may have found better ways to stabilize the movement of the callouts/labels more effectively and efficiently.

Upon critical review of the resulting animation, the following findings were made. To create a reasonably concise video output, the model was timed at 2 frames per minute and rendered at 30 frames per second. Therefore, the resulting animation was reasonably fast-paced. While this is justified given the speed at which the fire spread, certain important information can be missed. However, being an animation, it offers opportunities for review that static media does not such as the opportunity to slow down, fast forward, or rewatch. Also, animating the callouts/labels reduces the overall map load and the possibility of sensory overload from too many details shown at once. Throughout the animation, it is ensured that only what is viable within frame and at the appropriate time stamp is displayed

8.4 Possible Future Workflow

An additional future workflow could be leveraging wildfire modeling algorithms to statistically model the fire and then compare it in real-time, to test its efficiency and accuracy. Also, a further workflow may be developed that shows the real-time damage of 3D models of the structures as the fire consumes them. This may be done when more improvements are made to eth 3D photorealistic tiles that allow individual styling and material assignment to the buildings and structures in the model.

8.5 Limitations

Even though fires still occurred on subsequent days until August 15th, only the fires detected by the 375m spatial and limited temporal resolution VIRRS sensor could be visualized. This is a limitation of available remote sensing data to properly analyze the true extent of a fire.

The Aerosol Optical Depth (AOD) data which was originally intended to be used in modeling smoke plumes in this study could not be used also due to limitations in remote sensing data resolution.

8.6 Disclaimer

NASA Active fire points downloaded for this study contain some points observed over the sea. Because this is highly improbable, these points were manually moved to land to align with existing burn scars as observed from Maxar's 33cm satellite imagery.

9 CONCLUSION

This study aimed to create advanced 3D animation to retrospectively model a wildfire and assess the possibilities of integrating remote sensing and non-remote sensing data. Two separate detailed workflows were developed to achieve this at different resolutions. The first captured the fire progression across the entire island of Maui, and the other focused on the Lahaina fire. The workflows each involved acquiring the data, preprocessing, modeling, animation, rendering, and post-processing (video editing). This resulted in 5 separate animations depicting different views of the fire, as listed below.

- Overview Animation of Maui Island Fire
- Animation of Lahaina: South-western view
- Animation of Lahaina fire: Eastern hillside view
- Animation of Lahaina fire: Harbor View
- Lahaina Fire Animation: Aftermath (Damage and Historical Landmarks)

An evaluation of the resulting animation was done by comparing it to official records of the fire. The benefits and limitations of using the currently available Google Photorealistic 3d tiles in this study context were identified as well as critical issues with the speed and layout of the animation.

Furthermore, this study found that the VIIRS Deep Blue Aerosol 6 mins 6KM Swath data, with a sensor/algorithm resolution of 6 km at nadir, imagery resolution is 2 km at nadir, and the temporal resolution is daily, which is one of the best currently available Aerosol Optical Depth (AOD) products, could not be successfully integrated in the 3D modeling workflow to depict smoke plumes at the scale intended in this study (Maui Island). This is due to the incompatibility of its spatial and temporal resolution for this purpose.

REFERENCES AND INFORMATION SOURCES

Atwood, P. (2024). *Peter Atwood*. Peter Atwood. https://peteratwoodprojects.wordpress.com/

Avila-Flores, D., Pompa-Garcia, M., Antonio-Nemiga, X., Rodriguez-Trejo, D. A., Vargas-Perez, E., & Santillan-Perez, J. (2010). Driving factors for forest fire occurrence in Durango State of Mexico: A geospatial perspective. *Chinese Geographical Science*, *20*(6), 491–497. https://doi.org/10.1007/s11769-010-0437-x

Blender. (n.d.-a). *Blackbody Node—Blender 4.2 Manual*. Retrieved July 26, 2024, from https://docs.Blender.org/manual/en/latest/modeling/geometry_nodes/utilities/color/blackbody.html#index-0

Blender. (n.d.-b). *Geometry Nodes—Blender 4.2 Manual*. Retrieved July 26, 2024, from https://docs.Blender.org/manual/en/latest/modeling/geometry_nodes/index.html

Bowman, D. M. J. S., Williamson, G. J., Abatzoglou, J. T., Kolden, C. A., Cochrane, M. A., & Smith, A. M. S. (2017). Human exposure and sensitivity to globally extreme wildfire events. *Nature Ecology and Evolution*, *1*(3). https://doi.org/10.1038/s41559-016-0058

Campbell, & Wynne. (2011). *Introduction to Remote Sensing.* Guilford Press.

Castrillón, M., Jorge, P. A., López, I. J., Macías, A., Martín, D., Nebot, R. J., Sabbagh, I., Quintana, F. M., Sánchez, J., Sánchez, A. J., Suárez, J. P., & Trujillo, A. (2011). Forecasting and visualization of wildfires in a 3D geographical information system. *Computers and Geosciences*, *37*(3), 390–396. https://doi.org/10.1016/j.cageo.2010.04.011

Cattau, M. E., Wessman, C., Mahood, A., & Balch, J. K. (2020). Anthropogenic and lightning-started fires are becoming larger and more frequent over a longer season length in the U.S.A. *Global Ecology and Biogeography*, *29*(4), 668–681. https://doi.org/10.1111/geb.13058

Cesium. (2024). *The Cesium Platform*. Cesium. https://cesium.com/platform/

CNN. (2024, November 1). *Maui Wildfire Timeline: How the Lahaina Inferno Raged, Hour by Hour—The New York Times*. https://www.nytimes.com/interactive/2023/11/01/us/hawaii-maui-fire-timeline.html

domlysz. (n.d.). *GitHub—Domlysz/BlenderGIS: Blender addons to make the bridge between Blender and geographic data*. Retrieved July 26, 2024, from https://github.com/domlysz/BlenderGIS

Earth Science Data Systems, N. (2015, April 6). *Fire Information for Resource Management System (FIRMS) | Earthdata* [Basic Page]. Earth Science Data Systems, NASA. https://www.earthdata.nasa.gov/learn/find-data/near-real-time/firms

EOX. (n.d.). *Sentinel-2 cloudless map of the world by EOX*. Retrieved July 26, 2024, from https://s2maps.eu/#

Eui, K. (2022, March 22). *Maui Island Digital Zoning Map*. https://www.mauicounty.gov/DocumentCenter/View/127982/Maui-Island-Digital-Zoning-Map-3-

EUMETSAT. (2020, December 8). *Copernicus Sentinel-3 NRT Aerosol Optical Depth*. https://www.eumetsat.int/S3-AOD

Fire Safety Research Institute, Kerber, S., & Alkonis, D. (2024). *Lahaina Fire Comprehensive Timeline Report*. UL Research Institutes. https://doi.org/10.54206/102376/VQKQ5427

geoBoundaries. (n.d.). *geoBoundaries*. Individual Country Files. Retrieved July 26, 2024, from https://www.geoboundaries.org/countryDownloads.html

Haven, H. (n.d.). *Hilltop Sunset Sky Dome • HDRI Haven*. Retrieved July 26, 2024, from https://hdri-haven.com/hdri/hilltop-sunset-sky-dome

Hawaii DOAG. (2024). *Maui Wildfire Investigation Resource Page*. https://ag.hawaii.gov/maui-wildfire-investigation-resources-page/

Hu, J., Lv, Z., Yuan, D., He, B., & Yan, D. (2023). Intelligent Fire Information System Based on 3D GIS. *Virtual Reality and Intelligent Hardware*, *5*(2), 93–109. https://doi.org/10.1016/j.vrih.2022.07.002

Hwang, K., Harpold, A. A., Tague, C. L., Lowman, L., Boisramé, G. F. S., Lininger, K. B., Sullivan, P. L., Manning, A., Graup, L., Litvak, M., Lewis, G., Miller, K., Brooks, P. D., & Barnard, H. R. (2023). Seeing the Disturbed Forest for the Trees: Remote Sensing Is Underutilized to Quantify Critical Zone Response to Unprecedented Disturbance. In *Earth's Future* (Vol. 11, Issue 8). John Wiley and Sons Inc. https://doi.org/10.1029/2022EF003314

Jesse G. Wald (Director). (2023, December 6). *LAHAINA FIRE Recovery Update—December 2023 DRONE Video of Entire BURN-ZONE* [Video recording]. https://www.youtube.com/watch?v=y8_KMwXwewU

Kay, J. T. (2022, November 7). Blender UI | Layout. *Medium*. https://medium.com/@jordantkay/Blender-ui-layout-3e21ee4e3765

Kenan Proffitt (Director). (2023, June 11). *Geometry Nodes Tutorial: Draw Fire In Blender!* [Video recording]. https://www.youtube.com/watch?v=brDn-ks7Ld8

Kim, S., Jeong, Y., Youn, Y., Cho, S., Kang, J., Kim, G., & Lee, Y. (2021). A Comparison between Multiple Satellite AOD Products Using AERONET Sun Photometer Observations in South Korea: Case Study of MODIS, VIIRS, Himawari-8, and Sentinel-3. *Korean Journal of Remote Sensing*, *37*(3). https://doi.org/10.7780/kjrs.2021.37.3.14

Li, X., Li, J., & Haghani, M. (2024). Application of Remote Sensing Technology in Wildfire Research: Bibliometric Perspective. *Fire Technology*. https://doi.org/10.1007/s10694-023-01531-3

Lillesand, Kiefer, & Chipman. (2015). *Remote Sensing and Image Interpretation*. John Wiley & Sons.

Long-Fournel, M., Mattei, G., Morge, D., Blanpied, J., Esteve, R., Guerra, F., Ripert, C., & Jappiot, M. (2014). Spatio-temporal monitoring of burned area to evaluate post-fire damage: application on Fontanès wildfire (France). In *Advances in forest fire research* (pp. 1752–1754). Imprensa da Universidade de Coimbra. https://doi.org/10.14195/978-989-26-0884-6_193

Loría-Salazar, S. M., Sayer, A. M., Barnes, J., Huang, J., Flynn, C., Lareau, N., Lee, J., Lyapustin, A., Redemann, J., Welton, E. J., Wilkins, J. L., & Holmes, H. A. (2021). Evaluation of Novel NASA Moderate Resolution Imaging Spectroradiometer and Visible Infrared Imaging Radiometer Suite Aerosol Products and Assessment of Smoke Height Boundary Layer Ratio During Extreme Smoke Events in the Western USA. *Journal of Geophysical Research: Atmospheres*, *126*(11). https://doi.org/10.1029/2020JD034180

Lu, X., Zhang, X., Li, F., Cochrane, M. A., & Ciren, P. (2021). Detection of fire smoke plumes based on aerosol scattering using viirs data over global fire-prone regions. *Remote Sensing*, *13*(2), 1–22. https://doi.org/10.3390/rs13020196

Maui County. (2017). *County Profile, Mayor's Proposed Budget, Fiscal Year 2017*. https://www.mauicounty.gov/DocumentCenter/View/102556/010_06_County-Profile

Maui Police Department. (2024, January 23). *Preliminary After-Action Report: 2023 Maui Wildfire*. Maui Police Department. https://www.mauipolice.com/uploads/1/3/1/2/131209824/pre_aar_master_copy_final_draft_1.23.24.pdf

Maxar. (2023). *Maui Hawaii Fires | Maxar*. https://www.maxar.com/open-data/maui-hawaii-fires

NASA Applied Science. (2023, August 8). *Hawaii Wildfires Aug. 2023 | NASA Applied Sciences*. http://appliedsciences.nasa.gov/what-we-do/disasters/disasters-activations/hawaii-wildfires-aug-2023

NASA Data Viewer. (2023, August 8). *NASA Worldview*. https://worldview.earthdata.nasa.gov/?v=-158.03687643310172,20.15156194953692,-154.9474095194899,21.565556246587136&l=Reference_Labels_15m(hidden),Reference_Features_15m(hidden),Coastlines_15m,VIIRS_SNPP_AOT_Dark_Target_Land_Ocean,VIIRS_SNPP_AOT_Deep_Blue_Best_Estimate,VIIRS_NOAA20_AOT_Dark_Target_Land_Ocean(hidden),VIIRS_NOAA20_AOT_Deep_Blue_Best_Estimate(hidden),BlueMarble_NextGeneration,MODIS_Terra_CorrectedReflectance_TrueColor(hidden)&lg=true&t=2023-08-09-T00%3A00%3A00Z

NASA Disaster Portal. (2023). *Thermal Infrared Sensor (Landsat 8) on August 9, 2023 for the Hawai'i Wildfires—Overview*. https://maps.disasters.nasa.gov/arcgis/home/item.html?id=3b3b4e09fcc74d26b6a8a23473a96c78

NASA-FIRMS. (2023). *NASA-FIRMS Global Fire Map Viewer*. Global Fire Map Viewer. https://firms.modaps.eosdis.nasa.gov/map/

NASA-FIRMS. (n.d.). *Active Fire Data*. Retrieved July 26, 2024, from https://firms.modaps.eosdis.nasa.gov/map/

NBC News. (2023, August 15). *Timeline: How ferocious wildfires devastated Maui, hour by hour*. NBC News. https://www.nbcnews.com/news/us-news/maui-wildfires-timeline-fires-created-chaos-rcna99967

NESDIS,NOAA. (n.d.). *Visible Infrared Imaging Radiometer Suite (VIIRS)*. National Environmental Satellite, Data, and Information Service. Retrieved July 26, 2024, from https://www.nesdis.noaa.gov/our-satellites/currently-flying/joint-polar-satellite-system/visible-infrared-imaging-radiometer-suite-viirs

OAM. (2023). *OpenAerialMap Maui 33cm Satellite Imagery August 9th and 12th, 2023*. OpenAerialMap Browser. https://browser.openaerialmap.org/

Ordinance Survey UK. (2024, March 1). *Using Blender for Geospatial Projects | More than Maps*. https://docs.os.uk/more-than-maps/deep-dive/using-Blender-for-geospatial-projects

OSM,HUMDATA. (2020). *United States (Hawaii) Buildings (OpenStreetMap Export)—Humanitarian Data Exchange*. United States (Hawaii) Buildings (OpenStreetMap Export). https://data.humdata.org/dataset/hotosm_usa_hawaii_buildings?

PDC,FEMA. (2023, August 12). *Pacific Disaster Center (PDC) and the Federal Emergency Management Agency (FEMA) releases Fire Damage*. Maui County. https://www.mauicounty.gov/CivicAlerts.aspx?AID=12683

Peter Atwood (Director). (2023, October 14). *Heat and Smoke: The 2023 Canadian Wildfire Season Animated* [Video recording]. https://www.youtube.com/watch?v=IVOfilQYupc

Profit, K. (2024). *Motion Blend*. Motion Blend. https://www.motionblendstudio.com

QMS. (n.d.). *QuickMapServices: Discover, share and use geospatial data services*. Retrieved July 26, 2024, from https://qms.nextgis.com/geoservices/5075/

Sawyer, V., Levy, R. C., Mattoo, S., Cureton, G., Shi, Y., & Remer, L. A. (2020). Continuing the MODIS Dark Target Aerosol Time Series with VIIRS. *Remote Sensing*, *12*(2), 308. https://doi.org/10.3390/rs12020308

Scianna, A. (2013). Building 3D GIS data models using open source software. *Applied Geomatics*, *5*. https://doi.org/10.1007/s12518-013-0099-3

Shennan, K., Stow, D. A., Nara, A., Schag, G. M., & Riggan, P. (2023). Geovisualization and Analysis of Landscape-Level Wildfire Behavior Using Repeat Pass Airborne Thermal Infrared Imagery. *Fire*, *6*(6). https://doi.org/10.3390/fire6060240

Shi, Y. R., Levy, R. C., Remer, L. A., Mattoo, S., & Arnold, G. T. (2024). Investigating the Spatial and Temporal Limitations for Remote Sensing of Wildfire Smoke Using Satellite and Airborne Imagers During FIREX-AQ. *Journal of Geophysical Research: Atmospheres*, *129*(2). https://doi.org/10.1029/2023JD039085

Song, B., & Duveneck, M. J. (n.d.). *Wildfire visualization using GIS and forest inventory data*. https://www.researchgate.net/publication/228641456

Southall, R., & Biljecki, F. (2017). The VI-Suite: a set of environmental analysis tools with geospatial data applications. *Open Geospatial Data, Software and Standards*, *2*(1). https://doi.org/10.1186/s40965-017-0036-1

Statista. (2023, November 15). *Wildfire economic damages worldwide 1991-2023*. Statista. https://www.statista.com/statistics/1423714/economic-impact-due-to-wildfires-worldwide/

Stewart, S. I., Radeloff, V. C., Hammer, R. B., & Hawbaker, T. J. (2007). *Defining the Wildland-Urban Interface*.

Sundström, A.,(2021). Introduction to satellite data Contents of the lecture. Earth and Space Observation Centre, Finnish Meteorological Institute

Szpakowski, D. M., & Jensen, J. L. R. (2019). A review of the applications of remote sensing in fire ecology. In *Remote Sensing* (Vol. 11, Issue 22). MDPI AG. https://doi.org/10.3390/rs11222638

Tateosian, L., & Tabrizian, P. (2017). *Blending tools for a Smooth Introduction to 3D Geovisualization*. https://www.researchgate.net/publication/320383098

Tedim, F., Leone, V., Amraoui, M., Bouillon, C., Coughlan, M. R., Delogu, G. M., Fernandes, P. M., Ferreira, C., McCaffrey, S., McGee, T. K., Parente, J., Paton, D., Pereira, M. G., Ribeiro, L. M., Viegas, D. X., & Xanthopoulos, G. (2018). Defining extreme wildfire events: Difficulties, challenges, and impacts. *Fire*, *1*(1), 1–28. https://doi.org/10.3390/fire1010009

Thomas, A. S., Escobedo, F. J., Sloggy, M. R., & Sánchez, J. J. (2022). A burning issue: Reviewing the socio-demographic and environmental justice aspects of the wildfire literature. In *PLoS ONE* (Vol. 17, Issue 7 July). Public Library of Science. https://doi.org/10.1371/journal.pone.0271019

Thöny, M., Schnürer, R., Sieber, R., Hurni, L., & Pajarola, R. (2018). Storytelling in interactive 3D geographic visualization systems. *ISPRS International Journal of Geo-Information*, *7*(3). https://doi.org/10.3390/ijgi7030123

U.S.Drought Monitor. (2023, August 1). *Map Viewer | U.S. Drought Monitor*. https://droughtmonitor.unl.edu/Maps/MapViewer.aspx

USGS. (n.d.). *USGS National Map Downloader*. Retrieved July 26, 2024, from https://apps.nationalmap.gov/downloader/

VIIRS Atmosphere Science Team, S. (2023). *VIIRS/SNPP Dark Target Aerosol L2 6-Min Swath 6 km* [Dataset]. NASA Level 1 and Atmosphere Archive and Distribution System Distributed Active Archive Center. https://doi.org/10.5067/VIIRS/AERDT_L2_VIIRS_SNPP.002

vvoovv. (n.d.). *Import of Google 3D Cities*. GitHub. Retrieved July 26, 2024, from https://github.com/vvoovv/blosm/wiki/Import-of-Google-3D-Cities

White, J. C., Hermosilla, T., & Wulder, M. A. (2023). Pre-fire measures of boreal forest structure and composition inform interpretation of post-fire spectral recovery rates. *Forest Ecology and Management*, *537*. https://doi.org/10.1016/j.foreco.2023.120948

Wikipedia. (2024). Climate of Hawaii. In *Wikipedia*. https://en.wikipedia.org/w/index.php?title=Climate_of_Hawaii&oldid=1213249524

Wooster, M. J., Roberts, G., Perry, G. L. W., & Kaufman, Y. J. (2005). Retrieval of biomass combustion rates and totals from fire radiative power observations: FRP derivation and calibration relationships between biomass consumption and fire radiative energy release. *Journal of Geophysical Research Atmospheres*, *110*(24), 1–24. https://doi.org/10.1029/2005JD006318

Yang, Z., Li, J., Hyyppä, J., Gong, J., Liu, J., & Yang, B. (2023). A comprehensive and up-to-date web-based interactive 3D emergency response and visualization system using Cesium Digital Earth: taking landslide disaster as an example. *Big Earth Data*. https://doi.org/10.1080/20964471.2023.2172823

ATTACHMENTS

Bound attachments:

Attachment 1: Code Snippet for Active fire points ingestion into Blender.

Free attachments

Attachment 2 Poster

Attachment 3 Flash drive

Attachment 4 ArcGIS Storymap (https://arcg.is/0SzrrW)

Flash Drive structure

Folders:

- Adobe Premiere Pro
    - Damages and Historical Landmarks
    - Eastern hillside view
    - Harbor View
    - Maui Island Overview
    - South-western view
- Blender Project File
    - OGmaui_38.blend
- Data
    - Activefiredata.csv
    - burnedarea
    - burnedbuilding
    - historic sites
    - lahainaboundary
    - lahainabuildings
    - mauiboundary
    - zones
- Layouts
    - Inset.png
    - Maxar9th.png
    - Scalebar.png
    - Damaged_buildings.pdf
    - Historical_Landmarks.pdf

Attachment 1: Python script to ingest active fire point into Blender

This code snippet reads the active fire data from .csv format into Blender. The csv file has already been modified to contain the XYZ coordinates of each point as well as the frame value, and FRP values. The attributes to be used in Geometry Nodes are taken from this ingested dataset. This script is based on a file by Atwood 2024.

```
import bpy
import csv
import numpy
import mathutils


# Set Parameters

# Filepath to CSV
filepath = "D:\\opeyemi\\activefiredata.csv" #location of the csv

# Name of Blender Object
obj_name = "mauifireframed" #name of the csv in blender

# Initialize an empty dictionary to store attributes
attributes = {}

#Create empty list for vertex data
data = []
verts = []

# Read CSV File

with open(filepath, mode='r', encoding='utf-8-sig') as f:
    reader = csv.DictReader(f)
    # Dynamically create dictionary keys based on CSV headers
    for header in reader.fieldnames:
        attributes[header] = []


    # Populate the dictionary
    for row in reader:
        data.append(row)
        for key in attributes.keys():
            try:
```

```
    # Assuming all values are to be converted to float, adjust if necessary
                value = float(row[key]) if row[key] else 0.0
                attributes[key].append(float(value))
            except KeyError:
                print(f"KeyError: Column '{key}' not found in CSV headers.")

# Append placeholder values for vertex position

for row in data:
    verts.append(mathutils.Vector((float(0), float(0), float(0))))

#Create Mesh

mesh_data = bpy.data.meshes.new(obj_name + '_data')
obj = bpy.data.objects.new(obj_name, mesh_data)
bpy.context.scene.collection.objects.link(obj)
mesh_data.from_pydata(verts, [], [])

# Create attributes and populate with data

for key in attributes.keys():
    key_name = key
    print(key_name)
    val = numpy.array(attributes[key])
    obj.data.attributes.new(name=key_name+'_val', type='FLOAT', domain='POINT')
    obj.data.attributes[key_name+'_val'].data.foreach_set('value',val)
```